Journal of
Translational Medicine

RESEARCH

Open Access

The microtubule targeting agent ST-401 triggers cell death in interphase and prevents the formation of polyploid giant cancer cells

Juan Jesus Vicente[1*†] , Kainat Khan[2†], Grant Tillinghast[3], José L. McFaline-Figueroa[3], Yasemin Sancak[2] and Nephi Stella[2,4*]

Abstract

Microtubule targeting agents (MTAs) are commonly prescribed to treat cancers and predominantly kill cancer cells in mitosis. Significantly, some MTA-treated cancer cells escape death in mitosis, exit mitosis and become malignant polyploid giant cancer cells (PGCC). Considering the low number of cancer cells undergoing mitosis in tumor tissues, killing them in interphase may represent a favored antitumor approach. We discovered that ST-401, a mild inhibitor of microtubule (MT) assembly, preferentially kills cancer cells in interphase as opposed to mitosis, a cell death mechanism that avoids the development of PGCC. Single cell RNA sequencing identified mRNA transcripts regulated by ST-401, including mRNAs involved in ribosome and mitochondrial functions. Accordingly, ST-401 induces a transient integrated stress response, reduces energy metabolism, and promotes mitochondria fission. This cell response may underly death in interphase and avoid the development of PGCC. Considering that ST-401 is a brain-penetrant MTA, we validated these results in glioblastoma cell lines and found that ST-401 also reduces energy metabolism and promotes mitochondria fission in GBM sensitive lines. Thus, brain-penetrant mild inhibitors of MT assembly, such as ST-401, that induce death in interphase through a previously unanticipated antitumor mechanism represent a potentially transformative new class of therapeutics for the treatment of GBM.

---

†Juan Jesus Vicente and Kainat Khan share equal contribution.

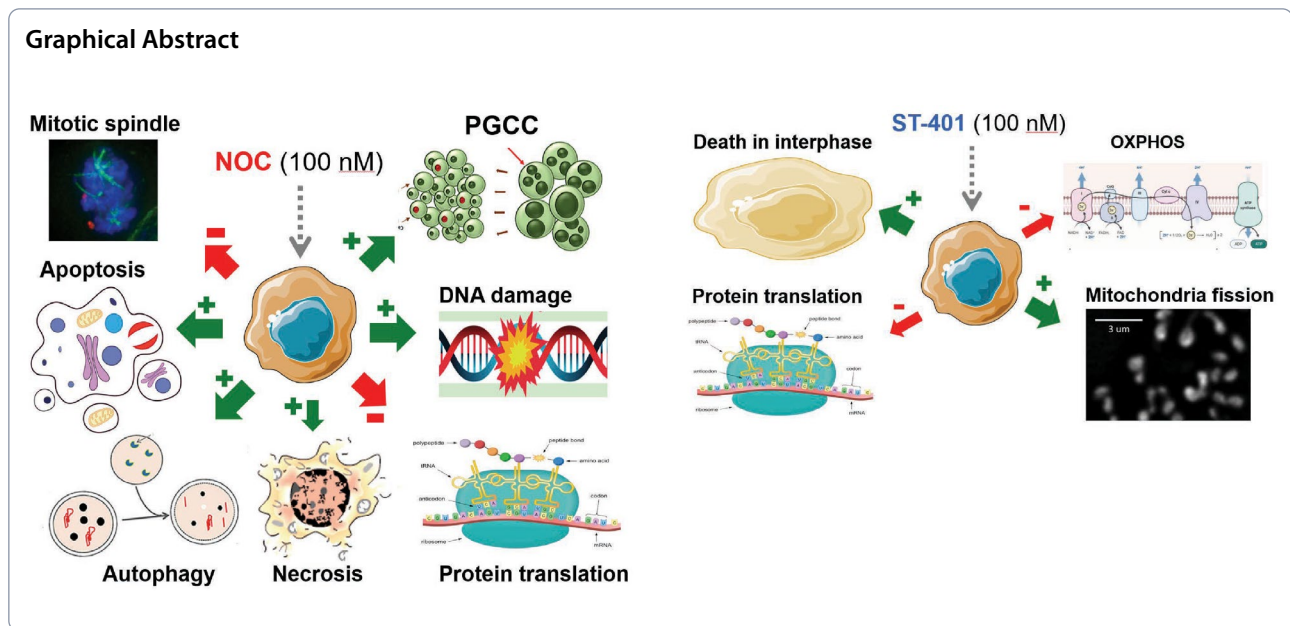*Correspondence:
Juan Jesus Vicente
jjvr@uw.edu
Nephi Stella
nstella@uw.edu
Full list of author information is available at the end of the article

Graphical Abstract

Introduction

Most MTAs bind directly to either tubulin dimers or assembled MTs, and depending on their mechanism of action (MOA), may inhibit either MT assembly or disassembly [1]. Structural biology studies have identified at least 7 ligand-binding sites on tubulin for MTAs, including sites targeted by inhibitors of MT assembly such as colchicine, vincristine and eribulin [2, 3]. In the case of MTAs that bind to the colchicine site of tubulin, it is well-know that they strongly inhibit MT assembly and ensuing dynamics within the spindle, which is essential to achieve error-free mitosis [4]. Thus, MTAs that target the colchicine site of tubulin will keep the spindle assembly checkpoint (SAC) activated and halt cell cycle progression of metaphase cells (metaphase arrest), resulting in delaying anaphase onset until all chromosomes have acquired proper attachments to MTs [5]. Consequently, extended metaphase arrest will ultimately trigger cell death by apoptosis, necrosis, and autophagy [5, 6]. Furthermore, the potential fate of cells upon mitotic slippage includes induction of senescence and quiescence [6]. Landmark studies demonstrated that most cancers exhibit slow doubling times and low mitotic indices (i.e., below 5%); and yet MTAs have proven remarkably efficacious antitumor agents [3, 5, 7]. This premise led the field to hypothesize that MTAs killing cancer cells in interphase may prove to be more efficacious and few examples have been reported [8, 9]; yet the molecular mechanism by which cancer cell die in interphase remains unknown.

SAC is frequently deregulated in cancer, and a significant portion of cancer cells treated with MTAs that bind to the colchicine site of tubulin escape SAC-induced death and exit mitosis with different levels of chromosome missegregation [5]. Such exit of mitosis produces daughter cells with different levels of aneuploidy, among them malignant polyploid giant cancer cells (PGCCs) [10]. Specifically, live cell microscopy revealed that mitotically arrested cells fail to undergo cytokinesis and exit mitosis through mitotic slippage to become PGCCs [10]. PGCCs carry devastating cancer-stem-cell features and are implicated in increased malignancy and enhanced metastatic characteristics, including drug resistance [11–15]. Furthermore, they are highly heterogenous and once formed activate the polyploid checkpoint and inactivate p53 signaling and other ploidy regulators [16]. Thus, the development of PGCCs following antitumor treatment is counter indicated. These studies favor the concept that killing cancer cells in interphase may represent a safer and more efficacious antitumor approach to reduce tumor mass than MTAs that target mitosis. However, understanding the mechanism involved in cell death in interphase has been difficult to resolve owing to the inability to experimentally isolate this event with selective compounds as means to identify the time course of this phenomenon.

In previous work, we developed a series of brain-penetrant small molecules (*ST-compounds*) that bind to the colchicine site of tubulin with high-affinity and mildly inhibits MT assembly as compared to NOC [17–20] (Fig. 1a). Key characteristics of ST-401, our recent and most potent ST-compound, are that it readily crosses the BBB and kills GBM cells with nanomolar potencies [20]. ST-401 exhibits significant in vivo anti-tumor activity in a preclinical GBM mouse model without inducing adverse
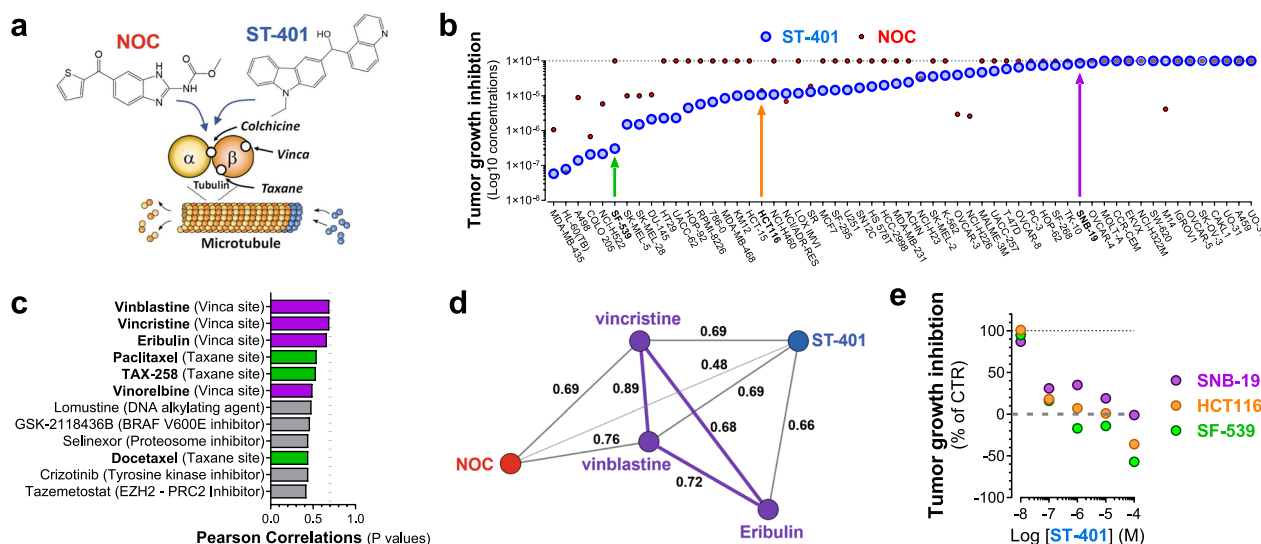
Vicente *et al. Journal of Translational Medicine*   (2024) 22:441

Page 3 of 20

Fig. 1 ST-401 and NOC kill cancer cells through a different antitumor mechanism: evidence from the NCI-60 cancer cell line panel. **a** Diagram illustrating ST-401 and NOC binding to the colchicine site of tubulin distinct from the vinca and taxane sites, all of which differentially influence MT dynamics via their binding to distinct sites on tubulin. **b** The antitumor activity of ST-401 was tested in the NCI-60 cancer cell line panel and results analyzed using COMPARE software. ST-401 exhibited significant antitumor activity in 46 out of 60 cancer cell lines as measured by total growth inhibition (TGI). SF-539 cells are highly sensitive to ST-401, HCT116 cells exhibited an average sensitivity and SNB-19 were much less sensitive to ST-401 (colored arrows). **c** The top 12 compounds with best correlations in antitumor activity (Pearson correlation) with ST-401. MTAs that target the vinca site (purple) or the taxane site (green) are among the top 12 (7 out of 12). Initial considerations of significance using COMPARE software is normally set at > 0.7 for Pearson correlation values (dotted line) and these values were not reached by these top 12 compounds. **d** Vector map representation of the direct Pearson correlations between ST-401 (blue) and its closest MTAs acting on the vinca site (purple) and nocodazole (NOC) (red). **e** Direct comparison of the antitumor activity of ST-401 measured in SF-539, HCT116 and SNB-19 cells within the NCI-60 panel shows differential sensitivities

effects, as measured by experimental toxicity [20]. These preclinical results underscore the therapeutic potential of ST-401 in Neuro-Oncology. Relevant to the current study, this milder response of ST-401 compared to NOC was established by showing that they inhibit MT assembly with comparable nanomolar IC_{50}s but different efficacies as measured by free tubulin released in biochemical assays and in cells in culture [17–20]. Together, these results showed that ST-401 is a milder inhibitor of MT assembly compared to NOC and raised the possibility that ST-401 might induce a different antitumor response than NOC.

In the current study, we analyzed the antitumor activity of ST-401 in the NCI-60 cancer cell line panel and identified 3 cancer cell lines that were differentially sensitive to ST-401 and NOC: 2 GBM lines, SF-539 and SNB-19, as well as HCT116 cells, a colorectal cell line commonly used to characterized the efficacy of MTAs at disrupting MT functions [21–25]. Thus, we first compared the MTA activities of ST-401 and NOC in HCT116 cells as reference model system and used live-cell microscopy imaging to identify the phase of the cell cycle when death occurs. We then performed a single cell RNA sequencing analysis of HCT116 cells treated with ST-401 and NOC to identify the molecular mechanisms that kill cancer cells in interphase and prevent the formation of PGCCs. We found that ST-401 induces a transient integrated stress response (ISR), greatly reduces energy metabolism as measured using Seahorse analysis, and promotes mitochondrial fission in interphase as measured by unbiased analysis of MitoTracker® staining, a combination of cellular responses that may underly death in interphase and avoid the development of PGCCs. A similar cell death mechanism characterized by pronounced reduction in energy metabolism and promotion of mitochondrial fission in interphase was detected in SF-539 GBM cells and was absent in SNB-19 cells, a GBM line less sensitivity to ST-401 treatment. Our study reveals a previously unanticipated antitumor mechanism that holds promises for the treatment of GBM.

Results

Distinct antitumor activities associated with ST-401 and NOC revealed by the NCI-60 cancer cell line panel analysis

We tested the antitumor activity of ST-401 in the NCI-60 cancer cell line panel and found that it significantly inhibited the growth of 47 out of 60 cancer cell lines as measured by total growth inhibition (TGI) (Log_{10} concentrations ranging from 58 nM to 860 µM),

Vicente *et al. Journal of Translational Medicine*   (2024) 22:441

Page 4 of 20

demonstrating that cancer cell lines exhibit differential sensitivities to ST-401 (Fig. 1b). The NCI-60 cancer cell lines were differentially killed by NOC (Fig. 1b), which was significantly less potent than ST-401. We further analyzed ST-401's antitumor activity using COMPARE to evaluate whether its antitumor activity correlated with any of the antitumor activity induced by > 100,000 chemical compounds and natural products tested on this panel thus far, including 169 compounds in the Approved Oncology Agents library [21, 25]. Figure 1c shows that the antitumor activity of ST-401 only poorly correlated with 12 FDA approved antitumor therapeutics, including MTAs that bind to the Vinca and Taxane sites, i.e., MTAs that bind to different sites on tubulin and affect MT dynamics via remarkably different MOA than MTAs that bind to the colchicine site (also see Additional file 1: Fig. S1c). Further analysis followed by vector representation of these results confirmed poor correlation with vincristine, vinblastine and eribulin (i.e., Pearson correlation > 0.7), and a remarkably different antitumor activity compared to NOC (Fig. 1d).

Results from the NCI-60 panel show that SF-539 cells are greatly sensitive to ST-401, and that HCT116 and SBN-19 cells are less sensitive (Fig. 1b). Concentration-dependent representations of their TGI responses indicated that ST-401 is more potent than NOC at killing these 3 cell lines, for example when tested at 100 nM concentrations (Fig. 1e). The GBM cell line, SF-539, expresses mutant p53, has a modal number at 88 chromosomes and divides every 35 h, whereas the GBM cell line, SNB-19, expresses wild type p53, has a modal number of 61 chromosomes and similarly divide every 35 h (Additional file 1: Fig. S1d). The colorectal cell line, HCT116, expresses wild type p53, is near diploid (modal number of 45 chromosomes) and divides every 17 h (Additional file 1: Fig. S1d). Thus, we sought to first study the differential antitumor activities of ST-401 and NOC in HCT116 as reference model system, and ultimately extend our results to SF-539 and SNB-19 cells to inform us on the relevance of their differential cellular response following acute treatments with ST-401 and NOC.

NOC profoundly disrupts the mitotic spindle and mitosis, whereas ST-401 predominantly leaves mitotic MT polymer intact, and this enables mitotic exit

It is well-known that NOC profoundly disrupts the mitotic spindle and arrests cells in mitosis prior to anaphase [26]. To determine the effects of ST-401 on the mitotic spindle and cell cycle arrest in more mechanistic details, we evaluated the appearance of tubulin polymer in fixed HCT-116 cells treated with ST-401 as compared to NOC, as well as scored the timing of cell division and cell death of treated cells by live microscopic analysis.

As expected, a 4 h treatment with NOC (50–200 nM) profoundly disrupted spindle morphology, inducing complete MT disassembly at 200 nM (Fig. 2a). By contrast, mitotic spindles remained provisionally intact during mitosis in HCT116 cells treated with ST-401 (50–200 nM) (Fig. 2a). Note that ST-401-treated HCT116 cells exhibited both congression defects in prometaphase and lagging chromosomes in anaphase at 50 and 100 nM, as well as multiple spindle poles at 200 nM (Fig. 2a, arrows). Thus, while HCT116 cells under control conditions exit mitosis in ≈ 40 min, HCT116 cells treated with NOC (100 nM) and ST-401 (100 nM) remained in mitotic arrest for approximately 10-20X longer (Fig. 2b). Figure 2a, b also show that ST-401-treated HCT116 cells exhibited congression defects and chromosome missegregation during anaphase that led to the formation of micronuclei (see arrow in Fig. 2b). Of note, many ST-401-treated cells exited mitosis despite apparent disruption of the mitotic spindle and lagging chromosomes identified during anaphase (Figs. 2c). In line with the stronger inhibition of MT assembly induced by NOC compared to ST-401, a 24 h treatment of HCT116 cells with NOC increased the mitotic index starting at 10 nM, whereas ST-401 increased their mitotic index at 100–300 nM (Fig. 2d). We also quantified the ability of HCT116 cells to successfully exit mitosis in the presence of NOC and ST-401 and found that most ST-401-treated cells were able to exit mitosis when compared to NOC (Fig. 2e). Of those cells that were able to exit mitosis, we then determined if HCT116-treated cells exit mitosis normally as determined by the absence of significant defects during anaphase. Specifically, abnormal mitotic exit was classified as cells presenting any of these phenotypes: chromosome missegregation, multipolar chromosome segregation, and mitotic exit without cytokinesis. Treatment with ST-401 reduced the number of HCT116 cells undergoing normal mitosis in a concentration dependent manner, with almost no effect at 50 nM and disruption of normal mitosis in 85% of cells at 200 nM (Fig. 2e, f). By contrast, NOC reduced the number of cells that undergo normal mitosis by 92–99% at all concentrations (Fig. 2e, f). Accordingly, Fig. 2g shows that most ST-401-treated cells successfully exited mitosis at all concentrations, and NOC treatment reduced the number of cells that were able to exit mitosis (i.e., they died in mitosis). These data enable 2 conclusions: (1) between 20 and 40% of cells treated with NOC at concentrations from 50 to 200 nM that entered mitosis will die during mitosis while the remaining 80–60% of the cells are able to exit; 2) A higher percentage of ST-401-treated HCT116 cells exit mitosis compared to NOC-treated HCT116 cells, and a higher percentage of these cells present a normal mitotic exit (i.e. no chromosome missegregation,
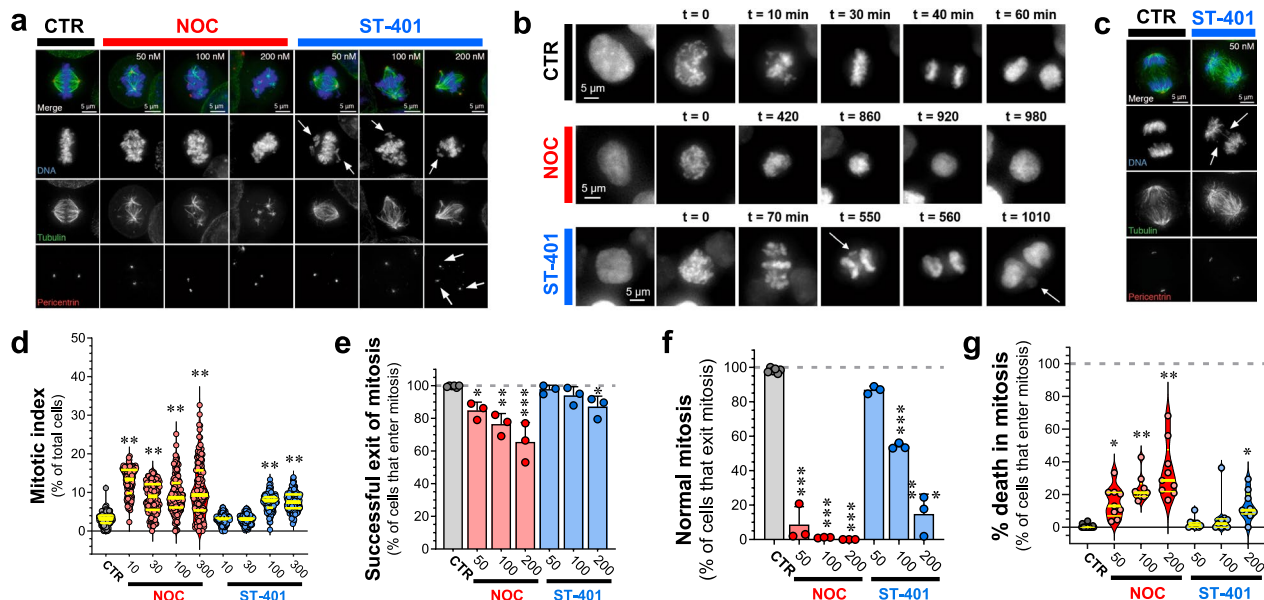
Vicente *et al. Journal of Translational Medicine*   (2024) 22:441

Page 5 of 20

Fig. 2 NOC profoundly disrupted the mitotic spindle and mitosis, whereas ST-401 predominantly left mitotic MT polymer intact, which enables mitotic exit. **a** Immunofluorescence images of HCT116 cells in mitosis after a 4 h treatment with either DMSO, NOC or ST-401. DNA was stained with DAPI (blue), MTs with an anti-tubulin antibody (green) and centrosomes with anti-pericentrin antibody (red). NOC had a more disruptive effect on spindles than ST-401. NOC eliminated a large amount of the MT polymer in the spindles. ST-401 cells showed congression defects (see arrows in DNA channel) and multipolar spindles at 200 nM (pericentrin channel). **b** HCT116 cells expressing histone H2B fused to mCherry were imaged for 24 h using live fluorescence microscopy in the presence of either vehicle or drugs (see Methods). The nuclear envelope breakdown to anaphase (or DNA decondensation) timing for CTR cells occurred around 40 min, while NOC (100 nM) and ST (100 nM) required several hours to exit mitosis. The NOC-treated HCT116 cell in this example exited mitosis without cytokinesis (just DNA decondensation without cell division, 920 min timepoint). The ST-401-treated HCT116 cells in this example presented congression problems (70 min time point) and lagging chromosomes in anaphase that become micronuclei (arrows in 550 min and 1010 min panels). **c** Immunofluorescence image of mitotic cells in anaphase after DMSO or ST-401 (50 nM) treatments. The immunofluorescence was performed as in panel a. ST-401 cells presented lagging chromosomes during anaphase (arrows). **d** Immunofluorescence of cells treated with DMSO, NOC or ST-401 for 24 h were analyzed to calculate the mitotic index (percentage of mitotic cells in a population). DAPI, anti-tubulin antibody and anti-pericentrin antibody were used to detect mitotic structures. We used CellProfiler to identify cells and its machine learning companion CellProfiler Analyst to quantify mitotic cells. NOC yielded a higher mitotic index at all concentrations after 24 h, while ST-401 induced such responses at 100 and 300 nM. For every condition, we recorded 50 random fields with a ×10 objective and an 18 mm diameter coverslip. Every spot in the graph corresponds to a field of view, and 3 independent experiments were performed and analyzed. **e** HCT116 cells tagged with H2B-mCherry were imaged for 24 h in the presence of either DMSO, NOC or ST-401. Most ST-401 treated cells exit mitosis, while a higher percentage of cells in NOC die during mitosis. Data are shown as mean ± s.e.m. of three independent experiments where a total of 2075 mitotic cells for ST-401 and 3317 mitotic cells for NOC were analyzed. **f** Of those cells that exit mitosis and exhibit feature of normal mitosis in the presence of NOC and ST-401 shown in **e**, ST-401 treatment of HCT116 cells at increasing concentrations resulted in a higher percentage of cells that exit mitosis without major defects as compared to NOC. **g** Of those cells that enter mitosis, NOC caused a higher percentage of cell death in mitosis at all concentrations. Statistics (**d-g**): ***$P < 0.001$, **$P < 0.01$ and *$P < 0.05$ significantly different from corresponding CTR (Two-way ANOVA followed by Dunnett's). For each, n = 3 independent experiments

no multipolar spindles and no exit without cytokinesis) compared to NOC.

Differential cell cycle responses: NOC treatment resulted in the development of polyploid cells while cells treated with ST-401 avoided this fate

To determine if NOC and ST-401 differentially affected the cell cycle, we analyzed the DNA content of HCT116 cells by flow cytometry using DAPI. As expected, short term treatment (i.e., 4 h) with NOC induced a stronger arrest in G2/M compared to ST-401; for example, NOC (100 nM) increased the number of HCT116 cells in G2/M

by twofold compared to control, while ST-401 (100 nM) increased the number of HCT116 cells in G2/M by 1.5-fold compared to control (Fig. 3a, b and Additional file 1: Fig. S3a for quantifications). The differential impact of NOC and ST-401 on the cell cycle was further amplified 24 h after treatment; for example, NOC (100 nM) reduced cells in G1 phase by 15-fold and reduced cells in S phase by fivefold as compared to CTR; whereas treatment with ST-401 (100 nM) did not affect the number of cells in G1 and S phases compared to CTR (Fig. 3c–f).

The increase in the number of cells presenting abnormal anaphases in NOC-treated cells compared
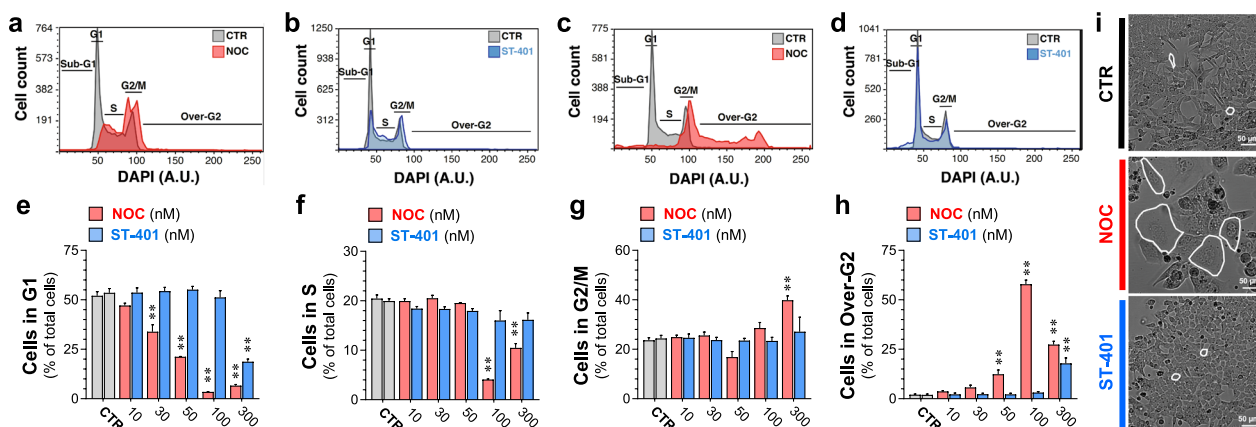
Vicente *et al. Journal of Translational Medicine*   (2024) 22:441

Page 6 of 20

Fig. 3 Differential cell cycle responses: NOC treatment resulted in the development of polyploid cells while ST-401 treatment did not. **a–d** Representative cell cycle plots of HCT116 cells treated with NOC (100 nM) and ST-401 (100 nM) for 4 h (a-b) or for 24 h (**c**, **d**). NOC increased the number of cells in G2/M after 4 h and in Over-G2 after 24 h, indicating the formation of polyploid cells, while ST-401-treated HCT116 cells underwent an unperturbed cell cycle (**b**). **e–h** Quantification of the number of HCT116 cells in each cell cycle phase when treated with DMSO (CTR) or with increasing concentrations of NOC and ST-401 for 24 h. NOC induced mitotic arrest and increased the number of polyploid cells at concentrations > 50 nM, whereas ST-401 induced this response only at 300 nM. Statistics (**e–h**) Data are expressed as mean ± s.e.m. of n = 3 independent experiments. **P < 0.01 significantly different from corresponding CTR (Two-way ANOVA followed by Dunnett's). **i** Representative bright field images of cells treated with NOC (100 nM) and ST-401 (100 nM) for 5 days. At the same concentration, NOC induced the formation of large polyploid cells

to ST-401-treated cells suggest different post-mitotic fates (see Fig. 2b–f). Accordingly, NOC-treated cells that exited mitosis without cytokinesis became polyploid as demonstrated by the increase in the number of cells referred to as "over-G2 phase" (e.g., from 2% of total cells in CTR conditions to 58% when treated with NOC (100 nM)) (Fig. 3c and h) [27, 28]. These polyploid cells in "over-G2" have an increased number of chromosomes and can be in S/G2/M phases of cell cycle as detected by the increase in DAPI fluorescence signal in values higher than the traditional diploid G2/M peak [29]. By sharp contrast, ST-401 treatment of HCT116 cells for 24 h at 100 nM did not generate polyploid cells and at 300 nM generated only 16% polyploid cells (Fig. 3d and h). Phase contrast microscopy showed that treatment with NOC (100 nM) for 5 days reduced HCT116 cell density and increased the presence of PGCC, whereas treatment with ST-401 (100 nM) had no such effect (Fig. 3i). Accordingly, a 24 h treatment with NOC (100 nM) increased cell size as measured by flow cytometry, whereas ST-401 (100 nM) did not (Additional file 1: Fig. S3b–d). Thus, a subset of HCT116 cells that arrested in mitosis in the presence of NOC eventually exited mitosis without completing cell division and persisted as PGCCs, while ST-401 treatment at the same concentrations avoided this fate.

NOC treatment of HCT116 cells induced apoptosis, autophagy, and necrosis, whereas ST-401 treatment avoided these fates and preferentially killed HCT116 cells in interphase

To further investigate the differential cell fate induced by NOC and ST-401, we used live-cell microscopy imaging during a 24 h treatment period to quantify the relative number of cells that died in mitosis versus interphase using the stable cell line HCT116-H2B-mCherry to fluorescently label chromosomes. Specifically, cells dying in mitosis versus interphase were scored based on chromatin condensation and increased DNA fluorescence observed during cell death (see representative images in Additional file 1: Fig. S4a). Figure 4a shows that, under vehicle-treated conditions, between 4 and 7% of HCT116 cells died in interphase (probably due to phototoxicity) [30]. Treatment with NOC at 50–200 nM killed 20–25% of HCT116-H2B-mCherry cells, whereas treatment with ST-401 at the same concentrations killed 8–20% of the cells (Fig. 4a). Thus, when considering the proportion of cells that died in mitosis versus interphase, ST-401 preferentially killed HCT116 cells in interphase as compared to NOC (e.g., 89% of the cells died in interphase with ST-401 at 100 nM compared to 53% of the cells dying in interphase with NOC at 100 nM (Fig. 4a). Moreover, ST-401 seems to preferentially kill cells in interphase before mitosis (Additional file 1: Fig. S4).
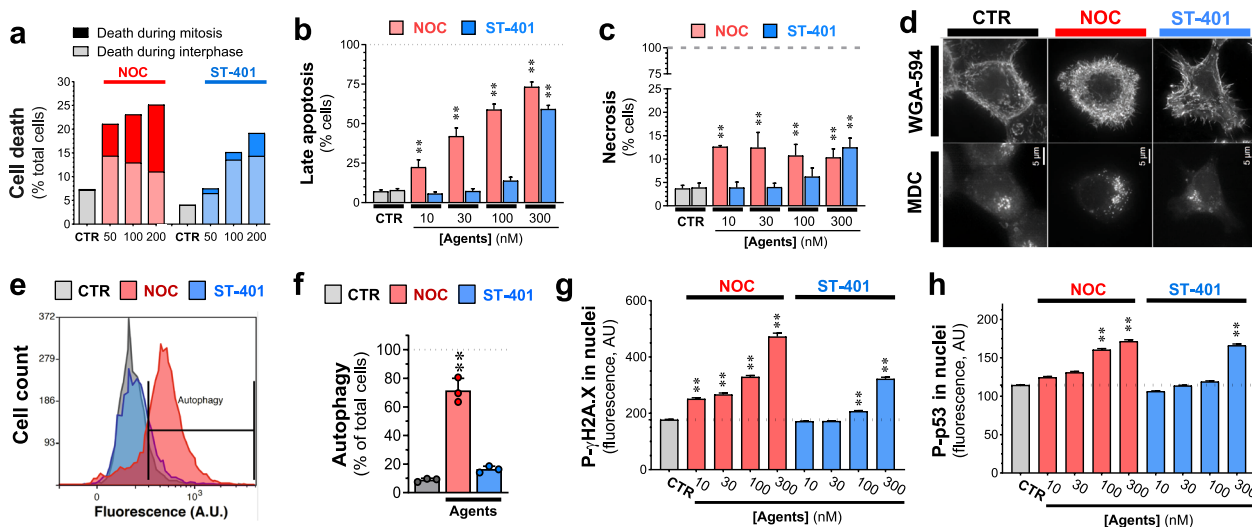
Vicente *et al. Journal of Translational Medicine*   (2024) 22:441

Page 7 of 20

Fig. 4 ST-401 kills preferentially in interphase whereas NOC kills preferentially in mitosis and induces apoptosis, autophagy, and necrosis. **a** Live-cell microscopy imaging of HCT116 cells treated with NOC and ST-401 for 24 h. NOC treatment results in comparable amounts of cell death in mitosis and interphase, while ST-401 treatment results in cells dying more frequently in interphase. Statistics (**a**). Data are shown as % of total cells from 3 independent experiments (5500 cells for ST-401 and 7200 cells for NOC). **b**, **c** HCT116 cells treated for 3 days with the MTAs, harvested, and labeled with PI/annexin V to measure apoptosis and necrosis using flow cytometry. NOC dose-dependently and gradually increases apoptosis levels whereas ST-401 induces an all-or-nothing increase in apoptosis at 300 nM. Statistics (**b**, **c**) Data are expressed as mean of 3 independent experiments with > 10,000 cells. Ordinary one-way ANOVA analysis. **P < 0.01 significantly different from corresponding CTR. **d**, **f** HCT116 cells stained with monodansylcadaverine (MDC) to detect autophagosomes in HCT116 cells treated with vehicle (CTR), NOC (100 nM) or ST-401 (100 nM) for 24 h. Fluorescence microscopy image of HCT116 cells (**d**). Flow cytometry histogram of MDC fluorescence (**e**). Quantification of MDC fluorescence by flow cytometry (**f**). NOC induces autophagy whereas ST-401 does not. Statistics (**e**, **f**): Data are expressed as mean ± s.e.m. of n = 3 independent experiments. **P < 0.01 significantly different from corresponding CTR (Two-way ANOVA followed by Dunnett's). **P < 0.01 significantly different from corresponding CTR. **g**, **h** HCT116 cells were treated vehicle (CTR), NOC (100 nM) or ST-401 (100 nM) for 24 h, immunostained for P-γH2AX and P-P53, imaged by fluorescence microscopy and pixel intensity analyzed. NOC increased the levels of both P-H2AX (**g**) P-P53 (**h**) in the nucleus in a concentration-dependent manner, whereas ST-401 only induced such response at higher concentrations. Statistics (**g**, **h**): Data are shown as median with 95% CI for 3 independent experiments where 23,000 and 10,000 total cells were measured for ST-401 and NOC, respectively. Ordinary one-way ANOVA analysis. **P < 0.01 significantly different from corresponding CTR

Based on this finding, we determined whether ST-401 induced cell death pathways frequently induced by NOC, such as apoptosis and necrosis [5]. We also checked for the accumulation of autophagosomes that could lead to death by autophagy [31]. To measure apoptosis and necrosis, we treated HCT116 cells with NOC and ST-401 for 1-, 3- and 5-days, and measured annexin-V (AV) (apoptosis) and propidium iodide (PI) (necrosis) staining by flow cytometry. Treatment with NOC and ST-401 for 1-day increased the number of cells in early and late apoptosis (e.g., 8% of CTR-treated cells were in late apoptosis and 17% and 13% of cells were in late apoptosis when treated with NOC (100 nM) and ST-401 (100 nM), respectively (Additional file 1: Fig. S4c–f). Neither drug induced necrosis in a 24 h treatment period (Additional file 1: Fig. S4c–f). Substantial differences between ST-401 and NOC emerged after 3 days treatments: as expected, NOC applied at 10 to 300 nM induced pronounced late apoptosis (e.g., 59% of NOC (100 nM)-treated cells were in late apoptosis) whereas ST-401 treatment induced late apoptosis only at 300 nM (i.e., 59% of total ST-401-treated

cells) (Fig. 4b and Additional file 1: Fig. S4d and f). NOC at 10 to 300 nM triggered necrosis after 3 days treatment, as shown by an increase of HCT116 cells that stained for PI and not for AV, (e.g., from 4% in CTR-treated cells to 13% in NOC (10 nM-treated cells) (Fig. 4c). By contrast, only ST-401 at 300 nM induced necrosis after 3 days in 13% of HCT116 cells (Fig. 4c). Thus, while ST-401 is more potent than NOC when measuring TGI inhibition in the NCI-60 cancer cell line panel, it is less potent than NOC at inducing apoptosis and necrosis, suggest an alternative cell death mechanism.

We then surveyed accumulation of autophagosomes labeled by the fluorescent biomarker monodansylcadaverine (MDC) [32]. Autophagy is a survival mechanism that enables cells to degrade damaged cellular components that are no longer needed and can potentially harm cells; however, cells eventually die when accumulating autophagosomes [33]. Figure 4d–f show that treating HCT116 cells for 24 h with NOC (100 nM) results in the accumulation of autophagosomes in 62% of the cells as detected by immunofluorescence (IF) microscopy and

Vicente *et al. Journal of Translational Medicine*   (2024) 22:441

Page 8 of 20

quantified by flow cytometry. ST-401 (100 nM), however, did not trigger the accumulation of autophagosomes (Fig. 4d–f). Interestingly, NOC treated cells that present high fluorescence values for MDC (i.e. accumulation of autophagosomes) also appear at high values of FSC-A and SSC-A, corresponding to increased size and complexity respectively (Additional file 1: Fig. S4h–j). Prolonged mitotic arrest leads to DNA damage, which triggers the intrinsic apoptosis pathway through p53 [34]. In fact, defects in chromosome segregation and DNA damage during anaphase trigger the phosphorylation and accumulation of phosphorylated p53 (P-p53) in nuclei in the subsequent interphase [35]. Figure 4g, h show that 24 h treatment with NOC increased in a concentration-dependent manner both P-γH2A.X levels, an index of DNA damage, and P-p53 levels in nuclei as measured by IF analysis, whereas only the highest level of ST-401 (300 nM) triggered such a response. Together, these results agree with the previous studies showing that NOC (100 nM) kills cancer cells by disrupting mitosis and inducing apoptosis, necrosis, and autophagy, as well as increasing nuclear DNA-damage and P-p53 accumulation. By contrast, lower concentrations of ST-401 do not cause this fate.

scRNAseq analysis reveals distinct mRNA signatures associated with NOC and ST-401 treatments, including signatures of apoptosis, hyperploidy, RNA/protein synthesis and mitochondrial function

The differential antitumor activities triggered by NOC and ST-401 at 100 nM provided an opportunity to identify the mRNA signatures associated with death in mitosis versus interphase, as well as the mRNA signatures associated with development of PGCCs. We performed scRNAseq analysis by single-cell combinatorial indexing RNA-seq (sci-RNA-seq3) of biological replicates to determine the mRNA signatures and cell state of HCT116 cells treated for either 8 h or 24 h with vehicle (CTR), NOC (100 nM) or ST-401 (100 nM) (Fig. 5a) [36]. In total, we analyzed the single-cell gene expression profiles of 214,165 cells after filtering cells based on both the total number of transcripts and the fraction of mitochondrial reads (Additional file 1: Fig. S5a–d). Quasi-Poisson regression analysis identified 2635 and 3280 genes that were differentially expressed (DEG) as a function of NOC or ST-401 exposure for 8 h and 24 h, respectively (FDR < 0.05, |normalized β coefficient| > 0.2) (Additional file 1: Fig. S5e, f).

As expected, α/β-tubulin genes exhibited tubulin autoregulation when treated with MTAs, as shown by both NOC and ST-401 affecting the expression of 6 TUB mRNAs, although ST-401 induced a milder response (Fig. 5b, c) [37, 38]. We First used the bioinformatic

platform Metascape to identify gene sets associated with biological pathways that are enriched within different modules (i.e., clusters) of differentially expressed genes following 24 h treatments with NOC and ST-401 (Additional file 1: Fig. S5g, h). Thus, Fig. 5d shows that both NOC and ST-401 induced a robust down-regulation of mRNAs related to the cell cycle and to RNA metabolism. Figure 5d also shows that both NOC and ST-401 induced a mild up-regulation in genes related to DNA damage and protein phosphorylation. Notably, ST-401 induced a pronounced down-regulation of mRNAs related to ribosomal assembly and function (ribosomal proteins) and protein translation, as well as those related to mitochondrial OXPHOS (oxidative phosphorylation) and function (Fig. 5d). In contrast NOC induced an opposite response (Fig. 5d).

We then used hierarchical clustering to group genes with similar dynamics across conditions. Our analysis showed that 8 h treatments with NOC and ST-401 led to the downregulation of most mRNAs, whereas 24 h treatments resulted in more complex changes in mRNA expression (Fig. 5e, f). Specifically, treatment of HCT116 cells for 8 h with NOC led to the upregulation of gene clusters related to G2/M check point regulation, p53 signaling and E2F targets, whereas ST-401 only mildly changed the expression of these gene clusters (Fig. 5e). Figure 5f shows that treatment of HCT116 with NOC for 24 h lead to the upregulation of gene clusters related to p53 signaling (Cluster 2) and a profound downregulation of EF2 targets (Cluster 5). Significantly, Fig. 5f shows that treatment of HCT116 cells with ST-401 for 24 h lead to the downregulation of the gene cluster related to OXPHOS and revealed a downregulation of MYC targets, many of which are associated with ribosomes and protein synthesis machineries (Clusters 6 and 1) [39]. Thus, NOC preferentially upregulated genes involved in p53 signaling, ST-401 preferentially downregulates OXPHOS genes, and NOC and ST-401 differentially regulate genes involved in protein translation.

To determine whether NOC and ST-401 induce distinct dynamic changes across cellular states, we performed dimensionality reduction using Principal Component Analysis (PCA) [40]. We accounted for batch effects between replicates and clustered cells using Leiden-based community detection, and further reduced dimensions using Uniform Manifold Approximation and Projection (UMAP) for visualization [41]. Analysis of the distribution of CTR, NOC and ST-401 clusters confirmed more complex cluster distributions between CTR, NOC and ST-401 treated for 24 h compared to 8 h (Additional file 1: Fig. S5i). Figure 5g highlights robust differences in the relative accumulation across cellular states following a 24 h treatment. Based on this premise,
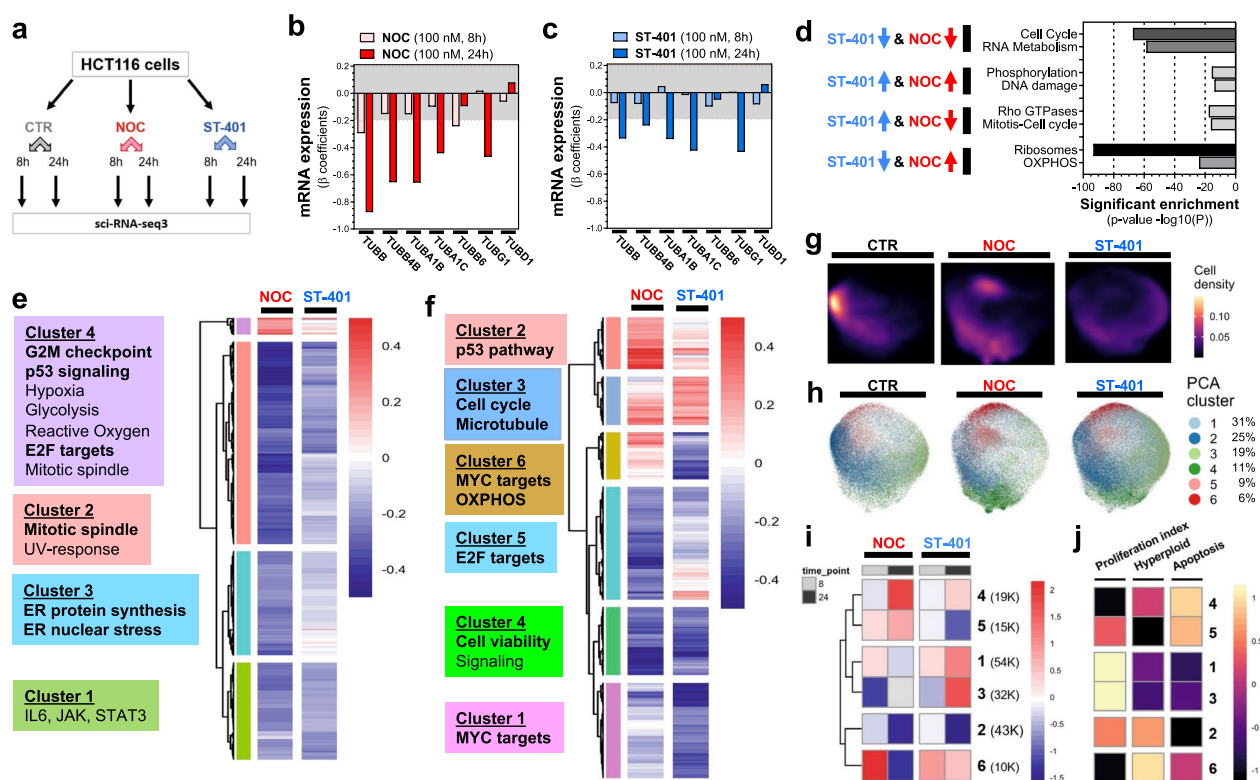
Fig. 5 ST-401 and NOC treatment induce differential gene expression and cell states. **a** Chart depicting the sample structure of our single-cell RNA-seq analysis of NOC and ST-401 exposed HCT116 cells. **b, c** Change in mRNAs that encode for tubulin subunits following 8 and 24 h treatments with NOC (100 nM) (**b**) and ST-401 (100 nM) (**c**). Both X and Y axis represent the normalized effect size (normalized β coefficient) relative to vehicle (CTR) in response to treatment. Statistics (**b, c**): Gray zone shows filtered for significance (from − 0.2 to 0.2). **d** Bioinformatic analysis using the platform Metascape reveals change in mRNA related to specific cell functions after 24 h treatments with NOC (100 nM) and ST-401 (100 nM) that follow the same and opposite directions. **e, f** Heatmaps of the union of differentially expressed genes (FDR < 0.05 & abs($\beta_{coefficient}$) > 0.2) as a function of NOC or ST-401 treatment for 8 h (**e**) or 24 h (**f**). Boxes to the right of each heatmap denote significant enriched gene sets for the highlighted gene clusters (FDR < 0.1, hypergeometric test). **g** UMAP embedding of single-cell transcriptomes of cells exposed to NOC, ST-401 or vehicle (CTR) for 8 h or 24 h faceted by treatment. Cells are colored by cluster and their relative abundance in % of total cells. h. Cell density by condition across the UMAP embedding from g. **g** Heatmap of the log2 of the odds ratio for the enrichment or depletion of cells across the cell state clusters from CTR treatment. Only statistically significant enrichments are shown (FDR < 0.05, Fisher's exact test). **h** Cell density analysis of transcriptomes of cells exposed to NOC, ST-401 or CTR for 24 h. UMAP embedding of single-cell transcriptomes of cells exposed to NOC, ST-401 or vehicle (CTR) for 8 h or 24 h. Colors denote Leiden-based community detection cluster assignments in PCA space as calculated using a mutual nearest neighbor approach clustered cells in PCA space with Leiden-based community detection. **i, j** Heatmap of the scaled aggregate expression of genes associated with proliferation, hyperploidy and apoptosis for the cell state clusters from **h**. Rows (clusters) are ordered as in i. Hyperploid and Apoptosis scores were derived from the MSigDB Chemical and Genetic perturbation and the Hallmark gene set collections, respectively

we investigated the relative accumulation of cells from our condition across 6 cellular states identified by Leiden community detection as a function of treatment time [42]. Figure 5h–j show the phenotypes induced by NOC and ST-401 that are correlated with cellular states as calculated by aggregate gene expression scores based on genes associated with proliferation, hyperploidy and apoptosis. After 8 h, NOC greatly increased scores for cluster 6 that is characterized by a reduced proliferation index, increased apoptosis and increased hyperploidy scores, and these scores were greatly decreased after 24 h treatment (Fig. 5i, j). By contrast, ST-401 induced a much milder such response (Fig. 5i, j). Furthermore, a 24 h treatment with NOC increased scores for cluster 4, which is also characterized by a reduced proliferation index, increased apoptosis and increased hyperploidy scores, whereas such response was much milder in ST-401-treated cells (Fig. 5i, j). Treatment for 24 h with ST-401 decreased scores for clusters 2 and 5 that involve genes related to the proliferation index (Fig. 5i, j). Together, our single-cell transcriptomic analysis reinforces our findings that NOC and ST-401 differentially affect proliferation, hyperploidy, and apoptosis and identified gene clusters involved in RNA/protein synthesis

and mitochondrial function as predominant differential responses.

Differential integrated stress responses (ISRs) induced by NOC and ST-401

Our scRNAseq analysis indicated that NOC and ST-401 differentially change the expression of genes related to ribosomal proteins and protein translation. We singled out mRNA encoding for ribosomal proteins and plotted the β-coefficients from the DEG tests distributed in quadrants to assess similar and opposite responses. Figure 6a, b confirm that mRNAs encoding for cytoplasmic ribosomal proteins are differentially regulated by NOC and ST-401, emphasizing that ST-401 treatment predominantly downregulated these mRNA after both 8 and 24 h treatments as opposed to NOC, which predominantly upregulated these mRNAs. These opposite responses on the expression of cytoplasmic ribosome mRNAs suggest differential effects on protein synthesis and ISR [43]. We singled out select mRNA encoding for regulators of protein synthesis and ISR, plotted their β-coefficients

from the DEG tests, and found that ATF4 mRNA (the transcription factor regulating ISR output) was downregulated to a greater extent by ST-401 than NOC, and that mRNAs coding for core molecular components of the ISR (eIF2a, EIF2AK2 = PKR, EIF2AK1 = HRI, EIF2AK3 = PERK and EIF2AK4 = GCN2) were differentially regulated (Fig. 6c, d).

We used the puromycin assay to measure protein synthesis levels in HCT116 cells following treatment with NOC (100 nM) and ST-401 (100 nM) and found that NOC reduced protein synthesis by 56% and 50% after 8 h and 24 h, respectively; whereas ST-401 reduced protein synthesis by 20% after 8 h and no longer affected protein synthesis after 24 h (Fig. 6e, f). In line with these results, 24 h treatment of HCT116 cells with NOC (100 nM) resulted in greatly increasing P-eIF2α levels as measured by western blot, whereas ST-401 (100 nM) treatment did not change the phosphorylation of this key regulator of protein synthesis (Fig. 6g). Increased P-eIF2α and development of stress granules play a key role in controlling protein
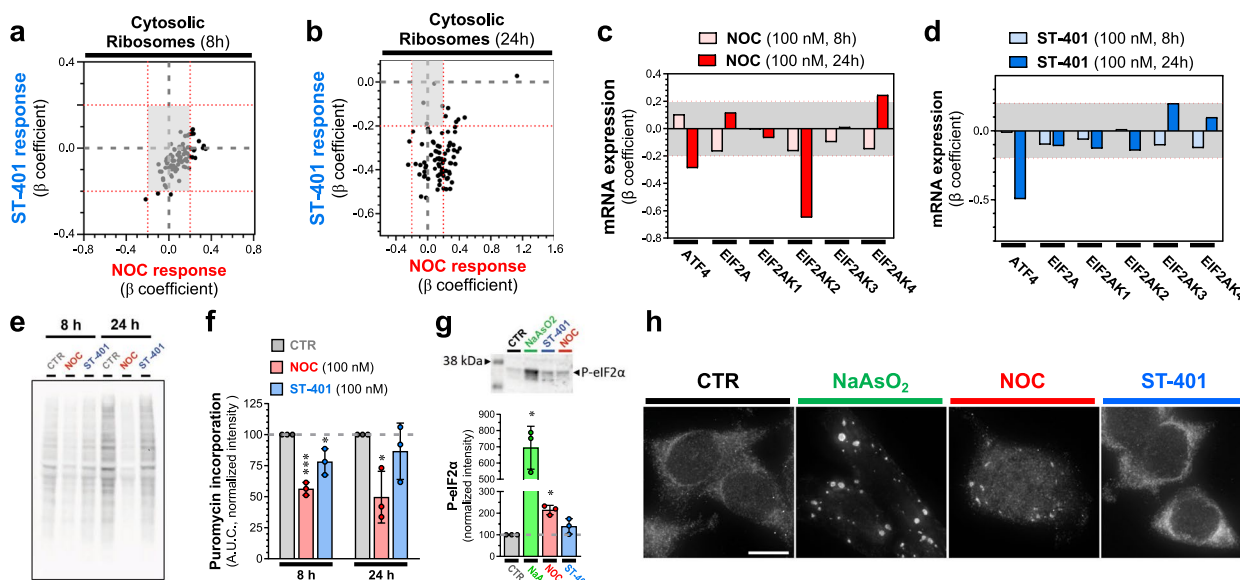

Fig. 6 NOC reduced protein synthesis and increased P-eIF2α levels, whereas ST-401 only induced such responses transiently. **a**, **b** Changes in the expression of mRNA coding for the cytosolic ribosomal machinery after 8 (**a**) and 24 h (**b**) treatment with NOC (100 nM) and ST-401 (100 nM). The x-axis represents the normalized effect size (normalized β coefficient) relative to vehicle (CTR) in response to treatment. **c**, **d** Change in the expression of mRNAs involved in the ISR following 8 h and 24 h treatments with NOC (100 nM) (**c**) or ST-401 (100 nM) (**d**). The x-axis represents the normalized effect size (β coefficient) relative to vehicle (CTR) in response to treatment. Statistics (**a**–**d**) Gray zone shows filtered for significance (from − 0.2 to 0.2). **e**–**f** Western blot analysis of puromycin staining of protein in CTR, NOC (100 nM) and ST-401 (100 nM) treated cells (e) and its quantification normalized by the total amount of protein using Ponceau staining (Additional file 1: Fig. S6a). Statistics (**e**, **f**): Data are expressed as means of 3 independent experiments. Ordinary one-way ANOVA analysis (followed by Tuckey). *P < 0.05 and **P < 0.01 significantly different from corresponding CTR. **g** Western blot analysis (top) and quantification (bottom) of P-eIF2α levels normalized by total amount of protein using Ponceau staining (Additional file 1: Fig. S6b). Statistics (**g**): Data are expressed as means of 3 independent experiments. Ordinary one-way ANOVA analysis (followed by Dunnett's). *P < 0.05 and **P < 0.01 significantly different from corresponding CTR. **h** Stress granules labeled with G3BP1 and visualized by fluorescence microscopy. Representative images of HCT116 cells treated for 24 h with vehicle (DMSO 0.1%, CTR), NOC (100 nM) or ST-401 (100 nM) and stained with G3BP1 to visualize stress granules. Positive control: NaAsO₂ (500 μM). Scale bar = 10 μM

Vicente *et al. Journal of Translational Medicine*   (2024) 22:441

Page 11 of 20

synthesis [44]. Figure 6h shows that 24 h treatment of HCT116 cells with NOC (100 nM) results in the accumulation of stress granules as analyzed by IF using G3BP1 as a marker [45]. Figure 6h also shows that the NOC response was less pronounced than the positive control NaAsO$_2$ and that ST-401 had no effect on this response [46]. Together, these results show that NOC induces a significant ISR characterized by pronounced and sustained reduction in protein synthesis, induction of ISR and formation of stress granule formation, whereas ST-401 only induces a transient ISR.

NOC and ST-401 differentially affect mitochondrial morphology and oxidative phosphorylation (OXPHOS)

Our scRNAseq analysis showed that NOC (100 nM) and ST-401 (100 nM) differentially regulate genes involved in mitochondria OXPHOS function. We singled out mRNA encoding for mitochondrial ribosomal proteins and plotted their β-coefficients from the DEG tests distributed in quadrants to assess similar and opposite responses. Figure 7a, b show that mRNAs encoding for mitochondrial ribosomal proteins are also differentially regulated by NOC and ST-401: ST-401 treatment predominantly downregulated these mRNA after both 8 h and 24 h treatments, as opposed to NOC that induced both up
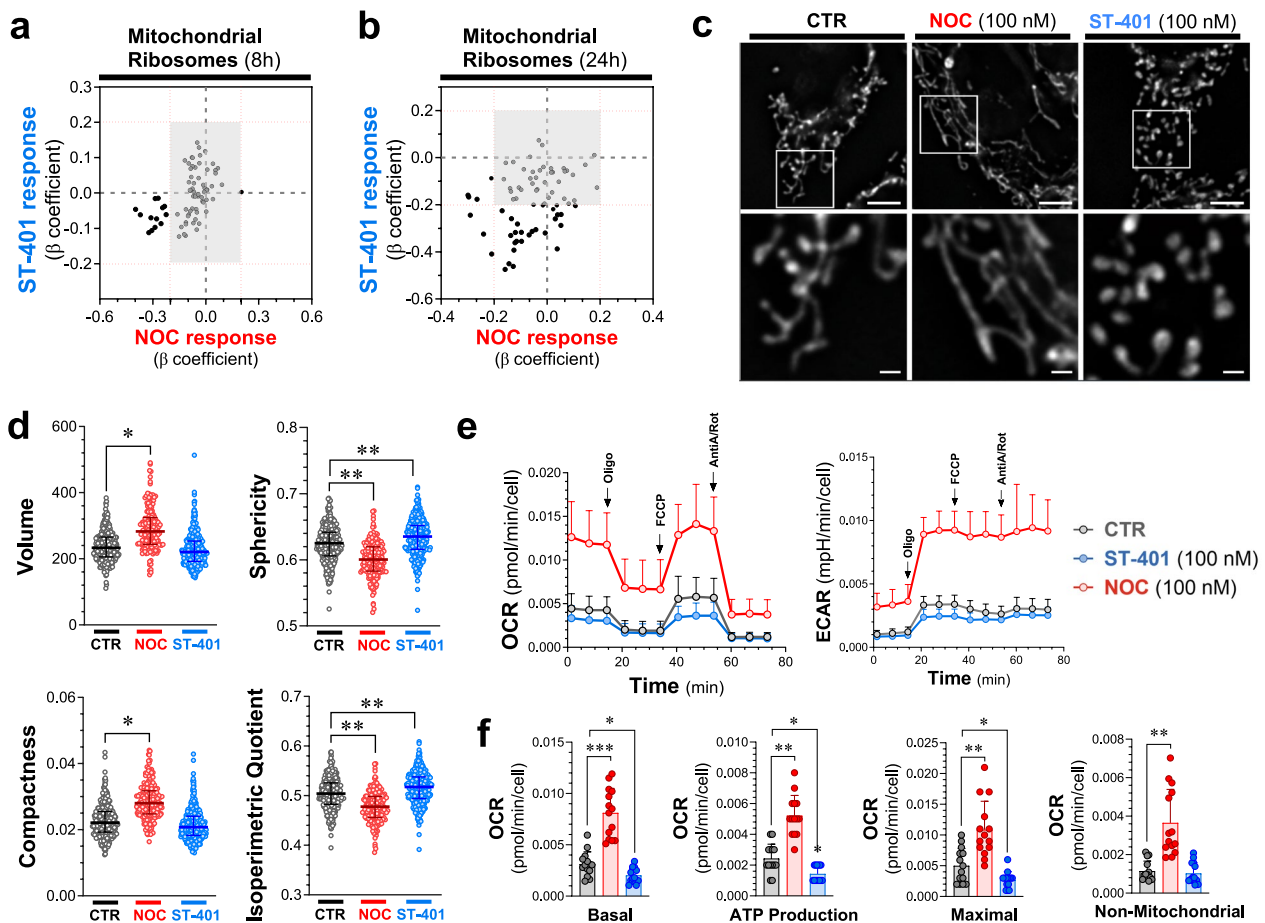

Fig. 7 Opposite changes in mitochondrial morphology and OXPHOS induced by NOC and ST-401. **a**, **b** Changes in the expression of mRNA coding for mitochondrial ribosomes after 8 (**a**) and 24 h (**b**) treatment with NOC (100 nM) or ST-401 (100 nM). The x-axis represents the normalized effect size (normalized β coefficient) relative to vehicle (CTR) in response to treatment. **c**, **d** Representative images of HCT116 cells treated for 24 h with vehicle (CTR), NOC (100 nM) or ST-401 (100 nM) and stained with mitoTracker to visualize mitochondria (c). Unbiased quantification of their volume, sphericity compactness and isoperimetric quotient (d). Statistics (**d**) Data are shown as mean ± s.e.m. of 3 independent experiments. Ordinary one-way ANOVA analysis resulted in * = p < 0.05 and ** = p < 0.01 compared to CTR. **e**, **f** Measure of the oxygen consumption rate (OCR) and of extracellular acidity response (ECAR) of HCT116 treated for 24 h with CTR, NOC (100 nM) or ST-401 (100 nM). Treatment with oligomycin (Olig, 1 μM), FCCP (1 μM), antimycinA/rotenone (1 μM) allowed to resolve the mitochondrial health based on the basal OCR, ATP production, maximal OCR response and non-mitochondrial respiration (**f**). Statistics (**f**) Data are shown as mean ± s.e.m. of 5 independent experiments. Ordinary one-way ANOVA analysis resulted in * = p < 0.05 and ** = p < 0.01 compared to CTR

and down-regulation of these mRNAs. These differential responses on mitochondrial ribosomal protein mRNAs suggest differential effects on mitochondrial function [47].

We analyzed mitochondrial morphology following a 24 h treatment of HCT116 cells with NOC (100 nM) and ST-401 (100 nM) stained with MitoTracker and measuring select parameters of their morphology using Mito-Map (a.k.a. MitoLoc) [48]. Figure 7c shows that NOC treatment induced a pronounced fusion of mitochondria whereas ST-401 induced a pronounced fission. Accordingly, NOC increased the volume and compactness of mitochondria, while reducing their sphericity and isoperimetry quotient (Fig. 7d). By contrast, ST-401 increased the sphericity and isoperimetric quotient of mitochondria without affecting their volume and compactness (Fig. 7d). To determine the impact of NOC and ST-401 on OXPHOS, we measured the oxygen consumption rate (OCR) and the extracellular acidification rate (ECAR) of HCT116 cells treated for 24 h. Figure 7e, f show that NOC treatment greatly increased overall OCR, including basal OCR by 2.7-fold and ATP-production by 2.2-fold, as well as several additional OCR parameters (Additional file 1: Fig. S7a). By contrast, ST-401 treatment greatly decreased basal OCR by 35% and ATP-production by 41%, as well as several additional OCR parameters (Fig. 7e, f and Additional file 1: Fig. S7a). NOC induced a comparable increase in ECAR as in its effect on OCR, and ST-401 induced a comparable decrease in ECAR as in its effect on OCR (Fig. 7e and Additional file 1: Fig. S7b). Of note, it is possible that the increased OCR of NOC-treated cells correlate with the increased cell size. Together, these results show that NOC and ST-401 treatments of HCT116 cells induces opposite changes in mitochondrial morphology, and OXPHOS and ECAR functions.
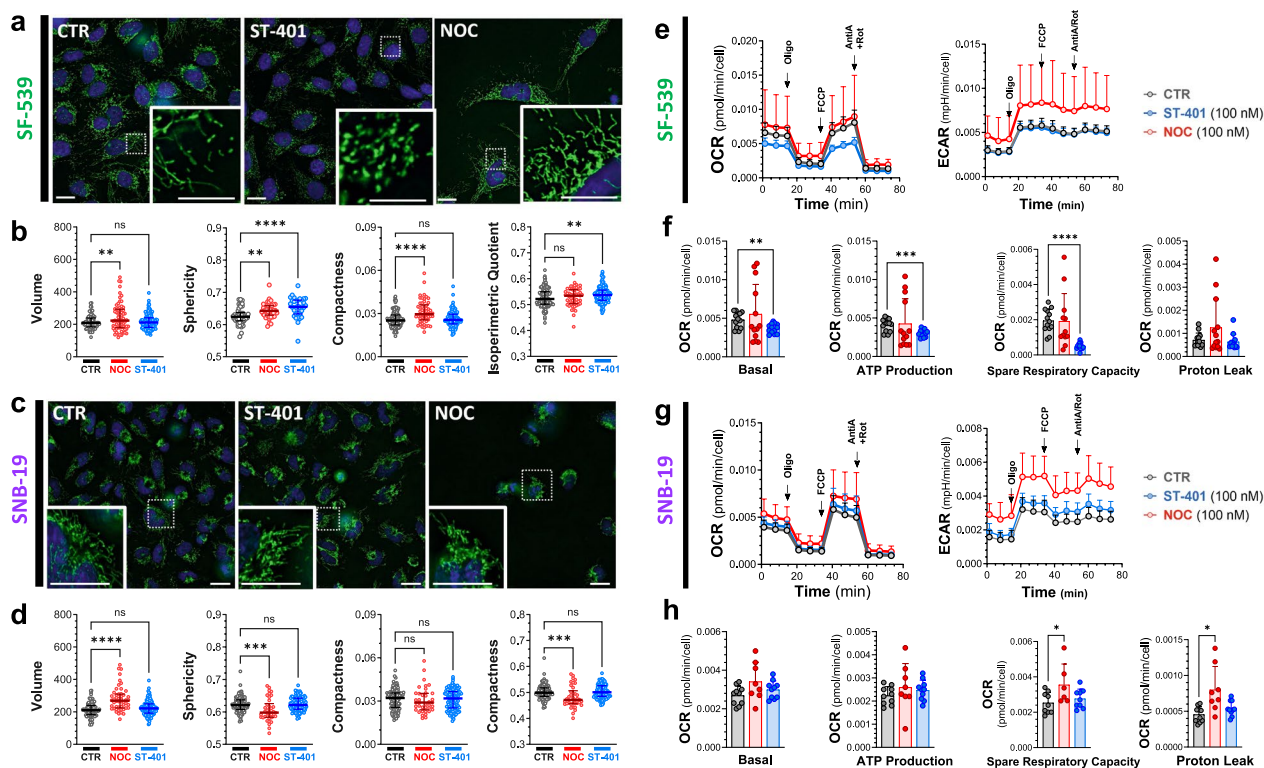
Considering that the most pronounced and opposite responses that we discovered in HCT116 treated with NOC (100 nM) and ST-401 (100 nM) were changes in mitochondrial morphology and OXPHOS function, we analyzed these mitochondrial readouts in the sensitive GBM cell lines, SF-539, and the less sensitive GBM cell line, SNB-19 (see Fig. 1e). Analysis of mitochondrial morphology in SF-539 cells stained with MitoTracker showed that NOC treatment also induced mitochondria fusion as indicated by concomitant increased in their volume, sphericity, and compactness, while unaffecting isoperimetry quotient; whereas ST-401 treatment induced a pronounced fission as indicated by increased in their sphericity and isoperimetry quotient, while unaffecting their volume and compactness (Fig. 8a, b). When analyzing SNB-19 cells, we found that NOC treatment induced a mild fission of mitochondria as indicated by increased

in their sphericity, compactness and isoperimetry quotient, while unaffecting their volume; whereas ST-401 treatment did not significantly affect their morphology (Fig. 8c, d).

Analysis of the OCR in SF-539 cells showed that ST-401 treatment decreased overall OCR, including basal OCR by 29%, ATP-production by 26%, non-mitochondrial ORC by 25%, spare respiration capacity by 73% and maximal OCR by 38% without affecting proton leak (Fig. 8e, f and Additional file 1: Fig. S8a). Remarkably, and as opposed to HCT-116 cells, NOC treatment of SF-539 did not increase OCR (Fig. 8e, f and Additional file 1: Fig. S8a). ECAR in SF-539 cells was increased by NOC and unaffected by ST-401 (Figs. 8e). When analyzing SNB-19 cells, we found that ST-401 did not affect OCR and that NOC treatment induced a trend to increased OCR that was variable and only reached significance when analyzing spare respiration capacity (+40%) and proton leak (+76%) (Fig. 8g, h and Additional file 1: Fig. S8b). ECAR in SNB-19 cells was increased by NOC and mildly affected by ST-401 (Figs. 8e). Together, these results show that NOC and ST-401 treatments of SF-539 cells induces opposite changes in mitochondrial morphology, and in OXPHOS and ECAR functions, similarly to its effect in HCT116 cells. In SNB-19 cells, NOC treatment induces mitochondrial fission with changes in OCR but increase in ECAR, whereas ST-401 does not affect mitochondrial morphology and OXPHOS function.

Discussion

The pronounced disruption of MT dynamics during mitosis induced by potent MTAs, such as NOC, delays the correct formation of MT-kinetochore attachments, which elicits the spindle assembly checkpoint and eventually induces cell death following prolonged mitotic arrest. This molecular mechanism, together with spindle defects that remain following MTA treatment, led the field to propose that MTAs primarily kill cancer cell in mitosis [49]. However, recent studies using drugs that target specific proteins involved in the mitotic machinery (e.g., selective inhibitors of kinases involved in mitotic spindle function) showed limited antitumor activities that never reached the significant antitumor activity achieved by current MTAs in the clinic [50]. We discovered that ST-401, a milder inhibitor of MT assembly than NOC, induces cell death in interphase at low nanomolar concentrations and cell death in mitosis at higher concentration. This antitumor activity is not mimicked by NOC, suggesting that milder inhibition of MT dynamics may hold broader antitumor activity, killing cancer cells at low concentrations in interphase and at high concentrations also in mitosis.

Fig. 8 Contrasting Mitochondrial effects of ST-401 on the sensitive SF-539 and the resistant SNB-19 cells. a-b) Representative images of SF-539 cells and SNB-19 cells **c-d**) treated for 24 h with vehicle (CTR), NOC (100 nM) or ST-401 (100 nM) and stained with mitoTracker to visualize mitochondria. Unbiased quantification of their volume, sphericity compactness and isoperimetric quotient using statistics, data are shown as median of 3 independent experiments. Welch's t-test analysis resulted in *=p < 0.05 and **=p < 0.01 compared to CTR. **e–f**) Measure of the oxygen consumption rate (OCR) and of extracellular acidification response (ECAR) of SF-539 cells and SNB-19 cells (**g-h**) treated for 24 h with CTR, NOC (100 nM) or ST-401 (100 nM). Treatment with oligomycin (Olig, 1 µM), FCCP (1 µM), antimycinA/rotenone (1 µM) allowed to resolve the mitochondrial health based on the basal OCR, ATP production, proton leak and spare respiratory capacity. Data are shown as mean ± s.d. of 4 independent experiments. Unpaired t-test resulted in *=p < 0.05 and **=p < 0.01 compared to CTR

How do MTAs induce death in mitosis versus exiting mitosis? Studies that used live microscopy imaging of cancer cell lines showed that cells within any given cell line exhibit multiple fates following prolonged arrest. Specifically, while some cells die in mitosis, others exit mitosis without dividing and return to interphase; and once back in interphase, some cells undergo cell-cycle arrest, others die, and others re-replicate their genomes [51]. Importantly, these studies showed that cell fate is not necessarily genetically predetermined and that duration of mitotic arrest does not dictate fate [51]. One possible mechanism is that DNA damage slowly accumulates during a protracted mitosis that, in the absence of efficient repair, eventually activates cell death pathways [51]. Despite this fundamental evidence, it remains unclear whether death in interphase represents a delayed response to damage incurred during mitosis or whether returning to interphase without successfully dividing creates a de novo damage signal. We show that HCT116 cells treated with low

nanomolar concentrations of ST-401 were able to exit mitosis. By contrast, this did not occur in HCT116 cells treated with low nanomolar concentrations of NOC, which increased the mitotic index and triggered cell death via apoptosis, necrosis, and autophagy. Accordingly, NOC was more potent at increasing P-p53 and P-γH2AX levels and inducing apoptosis than ST-401, and ST-401 only induced such response at higher concentrations. Of those cells that exit mitosis and escape cell death, near to 100% of the NOC-treated cells exhibited chromosomal defects as compared to ST-401. In fact, some cells were able to exit mitosis without cytokinesis. This was confirmed by flow cytometry as a 24 h treatment with NOC (100 nM) resulted in ≈60% of cells developing polyploidy. Thus, our study suggests that potent inhibitors of MT assembly induce death in mitosis, whereas milder inhibitors of MT assembly allow cells to exit mitosis and then kill cancer cells in interphase at low concentrations and kill cancer cells in mitosis at high concentrations.

Vicente *et al. Journal of Translational Medicine*   (2024) 22:441

Page 14 of 20

The low doubling times and mitotic index of most tumors (between 1 and 3%) indicates that therapeutic approaches that also kill cancer cells in interphase likely hold increased efficacy [7]. The interphase MT network presents a large surface area for protein–protein interactions, and, combined with the innate polarity of MTs, allows the trafficking of proteins and organelles through the cell via motor proteins, such as kinesin and dynein [52]. In addition to spatially organizing the cellular contents, this machinery also controls cellular function via several signaling pathways [53]. We show that ST-401 induces cell death in interphase at low nanomolar concentrations, suggesting that HCT-116 cells in G1 phase are susceptible to cell death. Of note, the mechanism described here appears to differ from the mechanism found in cells that have passed a putative "microtubule sensitivity checkpoint" mechanism in late G1/early S-phase, continue to cycle and die following mitotic arrest [54].

Striking differences exist in the death response triggered by ST-401, vincristine and eribulin. Notably, the latter two MTAs kill cells in G2/M at lower (< 30 nM) and at higher concentrations (> 100 nM) induce death in G1 phase through a p53-dependent mechanism [8, 54, 55]. Thus, while ST-401 kills cancer cells in interphase at lower concentrations and in mitosis at higher concentrations, vincristine and eribulin do the opposite, killing cancers cells in mitosis at low concentration and in interphase at high concentration [55]. Whether other MTAs, such as vincristine and eribulin, also induce a transient ISR and disruption of mitochondria function in interphase as ST-401, and whether such response varies depending on the type of cancer cells, remains to be determined.

The mechanism inducing cell death in interphase induced by MT assembly inhibitors is not fully understood. The heterogeneous response of cancer cells in interphase to different levels of damage or errors during mitosis suggests that they exhibit different responses to low vs high levels of chromosome missegregation, DNA damage or mitotic delays. In fact, missegregation of a single chromosome can activate p53 signaling even without DNA damage or delayed mitosis [35]. Chromosome segregation during mitosis is a highly regulated process carried out by the mitotic spindle, a multiproteic machinery combined with dynamic MTs and proper tuning of MT dynamics within the spindle is essential to avoid the mis-segregation of chromosomes during anaphase and polyploidy [56]. Specifically, cancer cells that exit mitosis with low levels of chromosome missegregation, and escape cell death, may continue through multiple cell cycles and increasingly fail to split chromosomes between daughter cells,

accumulating genetic material over several cell cycles and eventually generate PGCCs [10]. Accordingly, live tracking of cell fate experiments revealed that PGCCs arise quickly if mitotically arrested cells exit mitosis with failed cytokinesis [11, 13, 14, 57, 58]. Possibly, the strong disruption of mitosis triggered by NOC that eliminates most MT polymer might favor the selection of cells that carry the ability to replicate without a spindle, a hallmark of PGCCs [16]. By contrast, ST-401 triggers low levels of chromosome missegregation and thus does not kill cells in mitosis. Together, these studies raised the possibility that killing cells by mitotic arrest may lead to the formation of malignant PGCCs and the killing cancer cells in interphase might be more efficient [7, 9, 50]. Potential outstanding questions include: Do enlarged PGCC require the upregulated autophagosome to recover in interphase? Could this be a therapeutic target to test in future experiments? Does combination with autophagy/modulating agents such as hydroxychloroquine or bortezomib eradicate PGCC?

Our scRNAseq analysis unraveled potential mechanisms associated with cell death in interphase that involve the ISR and impaired mitochondrial function. Cells respond to different types of stress by inhibition of protein synthesis and subsequent assembly of stress granules, which are cytoplasmic aggregates that contain stalled translation preinitiation complexes [59]. Specifically, the rate of protein synthesis in cells is tightly regulated, including through eIF2α. For example, in response to various forms of stress, cells reduce global translation, by which they prevent further protein damage, reallocate their resources to repair processes, and ensure cellular survival [60]. Thus, the packaging of cytoplasmic mRNA into discrete RNA granules regulates gene expression by delaying the translation of specific transcripts. Following translation, however, newly inactivated mRNAs released from polysomes can also be packaged into dynamic, transient structures known as stress granules. Protein synthesis is essential for the formation and growth of several types of cancer and often dispensable for non-malignant tissue homeostasis, and such tumors are often therapeutically vulnerable to protein synthesis inhibitors [61]. Autophagy is a regulated process for the degradation of damaged organelles or proteins activated by different types of stresses [5, 31, 62]. The damaged organelles or proteins are stored in autophagosomes that fuse to lysosomes for the elimination of those harmful components. Thus, autophagy allows cells to survive mild stressful conditions. We found that NOC induces prolonged ISR and autophagy, whereas ST-401 induces a transient ISR that does not result in the accumulation of stress granules and induction of autophagy after a 24 h treatment. Thus, the cell death mechanism induced by ST-401 in

Vicente *et al. Journal of Translational Medicine*   (2024) 22:441

Page 15 of 20

interphase does not involve autophagy despite a transient ISR.

Opposite changes in mitochondria morphology and OXPHOS: Converging lines of evidence indicate that mitochondria play a key role in the biological embedding of adversity, including linking the consequence of stress exposure to changes in mitochondrial structure and function [63]. This molecular link and its reprogramming are now recognized hallmarks of cancer as recent studies have uncovered remarkable flexibility in the specific pathways activated by tumor cells to support these key functions [64]. Thus, tumors reprogram pathways of nutrient acquisition and metabolism to meet the bioenergetic, biosynthetic, and redox demands of malignant cells [65]. Impairment of mitochondrial function by the ISR can lead to several problems for cancer cells, including reduced cell growth and increased cell death linked to reduced ATP levels. We found that NOC and ST-401 induce opposite responses on mitochondria morphology and OXPHOS: NOC induced mitochondrial fusion and increased mitochondrial volume and increased OXPHOS, whereas ST-401 induced mitochondrial fission without a changed volume and decreased OXPHOS. The mitochondrial phenotype induced by NOC is likely associated with increase superoxide production and contributes to the killing of HCT116 cells by apoptosis, necrosis, and autophagy [66]. The mitochondrial phenotype induced by ST-401 characterized by a reduction in energy metabolism is likely to contribute to the killing of HCT116 cells in interphase. Importantly, while most mitochondrial proteins are synthesized in the cytoplasm, select mitochondrial proteins, such as mitochondrial ribosomal proteins (MRPs), are synthesized in the cytosol and transported to mitochondria [67]. In fact, MRPs are elevated in select cancers and several approaches have been developed to target MRPs for the treatment of cancer [67, 68]. Considering that NOC and ST-401 differentially affect MRP expression, these results suggest that NOC and ST-401 treatment might also directly affect mitochondrial function independently of ISR, including by differentially affecting MRP expression directly. Thus, our results suggest that death in interphase induced by mild inhibition of MT assembly in interphase is likely to involve significant reduction in energy supply.

Might ST-401 help in the immune response against cancer cells? Natural killers (NK) are a type of effector lymphocyte with cytotoxic functions and part of the innate immune system [69]. They are present at high levels in the circulatory system and have the ability to detect and lyse infected, damaged, stressed or transformed cells [70, 71]. Specifically, NK detect the lack of MHC-I molecules (HLA-A, HLA-B, HLA-C, HLA-E, HLA-F, HLA-G) at the surface of transformed cells,

which triggers their cytotoxic activity [70, 71]. Our scRNAseq data shows that ST-401 downregulates HLA-A, HLA-B, HLA-C and HLA-E genes, while NOC does not affect HLA-A and HLA-C, upregulates HLA-B and downregulates HLA-E (Additional file 1: Fig. S9a, b). This result suggests that ST-401 could empower NK cells' activity at killing cancer cell [72]. Furthermore, ST-401 could also help the immune response against cancer cell activating the cGAS-STING pathway. This defense mechanism system detects the presence of DNA in the cytoplasm of cells, and activate an immune response to kill and clear potential cancer cells [73, 74]. It remains to be determined in cancer cells treated with ST-401 that present low levels of chromosome missegregation might trigger the cGAS-STING pathway, which would also complement its tumor killing activity.

In conclusion, our study unravels a molecular mechanism that mediates the death of cancer cells in interphase and involves impaired mitochondrial function characterized by fission and reduction in energy metabolism. Mild inhibition of MT assembly is likely to induce broad antitumor activity, killing cancer cells in interphase at low concentrations and in mitosis at high concentrations as compared to strong inhibition of MT assembly that principally kills cancer cells in mitosis and might lead to the development of PGCC.

Methods
Statistical analysis
GraphPad Prism 9: curve fit (three parameters), Multiple comparison (ANOVA followed by DUNETT's or TUCKEY's).

NCI-60 screen and COMPARE
The NCI-60 cell line screen is a service available to the cancer research community. The screening process, data processing, and the COMPARE algorithm are described: https://dtp.cancer.gov/databases_tools/docs/compare/compare_methodology.htm Briefly, cells are established in 96 well plates for 24 h, exposed to test compounds across a range of concentrations for 48 h and viability determined by sulforhodamine B dye exclusion assay. Data sets are created for the concentrations at which compounds caused 50% growth inhibition (GI50), total growth inhibition (TGI) or 50% cell kill (LC50). The compare algorithm works with the sets of data, returning either every possible pairwise correlation within a defined set of data (grid COMPARE) or uses a data set (seed) to determine the highest correlations within a defined set (targets) of data (standard COMPARE).

Vicente *et al. Journal of Translational Medicine*   (2024) 22:441

Page 16 of 20

Cell culture

The cell line-HCT 116 was purchased from ATCC, and SF-539 and SNB-19 were purchased from NCI, and cultured in RPMI media with 10% FBS, supplemented with 1X L-glutamine and 1% penicillin/streptomycin. Cells were maintained at 37 °C and 5% CO_2. When cells were 70–80% confluent they were subcultured using trypsin–EDTA.

Cell fixation and immunofluorescence

HCT116 cells were treated with NOC or ST-401 and were fixed after 4 h using 2% paraformaldehyde in methanol at −20 °C for 10 min. Tubulin and centrosomes were labeled using anti-tubulin monoclonal DM1-alpha (1:500, Sigma) or anti-pericentrin (1:500, Abcam) antibodies applied overnight at 4 °C. Alexa-fluor 488 and 647 secondary antibodies against mouse and rabbit IgG, respectively, were used to detect the anti-tubulin and anti-pericentrin antibodies. Coverslips were mounted using ProLong® Diamond containing DAPI (Molecular Probes, Eugene, OR) and cured for 24 h. Fluorescent images were collected as 0.5-µm Z-stacks on a Deltavision microscope system (Applied Precision/GEHealthcare, Issaquah, WA) using a 60 × 1.42 NA lens (Olympus, Tokyo, Japan). Images were deconvolved using SoftWorx 5.0 (Applied Precision/GEHealthcare), and representative images are presented as a flat Z-projection. Figure 4c, d: HCT116 cells were treated with NOC or ST-401 and were fixed with 4% paraformaldehyde in PBS at 37 °C for 15 min and permeabilized in 0.5% Triton X-100 for 5 min at room temperature. P-p53 and P-γH2AX were labeled using a mouse anti-P-p53 (1:250, Phospho-p53 (Ser15) (16G8), Cell Signaling Technology) or a rabbit anti-P-H2AX (1:250, Phospho-Histone γH2A.X (Ser139) (20E3), Cell Signaling Technology) applied overnight at 4 °C. Alexa-fluor 488 and 568 secondary antibodies against mouse and rabbit IgG, respectively, were used to detect the anti-P-p53 and anti-P-γH2AX antibodies. Coverslips were mounted using ProLong® Diamond containing DAPI (Molecular Probes, Eugene, OR) and cured for 24 h. Fluorescent images of random fields of the coverslips were collected using a GE InCell 2500. Automatic identification of nuclei and fluorescence intensity was performed using the free software CellProfiler.

Live-cell imaging

For live-cell imaging, a stable cell line HCT116-mCherry-H2B cells were cultured in glass-bottom 24 multi-well plates from Ibidi. Cells were switched to 37 °C in a CO_2 independent media (10% FBS) with either DMSO, NOC or ST-401. Live-cell images were acquired using a GE InCell 2500 system with a 20X lens. Time-lapse images were collected as 15 µm Z-stack series, with 3 µm Z-spacing, and with 10 min time intervals for 24 h. Images were deconvolved using the InCell software and processed with Fiji. All quantification was done manually using Fiji.

Cell cycle experiments

HCT116 cells were treated with either DMSO, NOC or ST-401 at different times. After drug treatment, cells were collected using trypsin and centrifuged at 1,000 r.p.m. (161 RCF) for 10 min. The cell pellets were resuspended in 400 µL of a 10 µg/mL DAPI, 0.1% NP40 Tris buffer. Cells were processed by flow cytometry, and cell cycle data was analyzed using FlowLogic software.

Apoptosis/necrosis experiments

HCT116 cells were treated with either DMSO, NOC or ST-401 at different times. After drug treatment, cells were collected using trypsin and centrifuged at 1,000 r.p.m. (161 RCF) for 10 min. To detect apoptosis and necrosis, cells were treated with a necrosis/apoptosis kit from ThermoFisher containing PI and Annexin V Alexa Fluor™ 488 according to the manufacturer specifications. Cell pellets were resuspended in 100 µL of annexin binding buffer, followed by treatment with 5 µL Alexa fluor annexin V-488 and 1 µL of 100 µg/mL PI. After 15 min at room temperature, 400 µL of buffer was added to the mix. Cells were processed by flow cytometry, and apoptosis/necrosis data was analyzed using FlowLogic software.

PI and Annexin V staining

PI is an impermeable DNA-binding dye that enters cells when the cell membrane is compromised. PI, when excited, emits light at around 620 nm (orange/red) and it is routinely used in flow cytometry as a necrosis marker. Annexin V is a phosphatidylserine-binding protein that is used as an apoptosis marker, and when fused to AlexaFluor 488, emits light at around 525 nm (green).

Puromycin incorporation

HCT116 cells were treated with either DMSO, NOC or ST-401 at different times. After drug treatment, cells were treated with 1 µM Puromycin (Thermo Scientific Chemicals) at 37 °C for 30 min. After Puromycin treatment cells were collected using trypsin and centrifuged at 1,000 r.p.m. (161 RCF) for 10 min. The cell pellets were resuspended in 100 µL of RIPA buffer with protease inhibitors and incubated in a rocking platform shaker at 4 °C for 60 min. After it, the samples were centrifugated at 12,000 r.p.m. (11,750 RCF) at 4 °C for 30 min. The supernatant was used for a western-blot experiment using a mouse-anti-Puromycin antibody (1:5000, Millipore MABE343). To detect primary Ab, we incubated samples with donkey-anti-mouse Ab fused to HRP

(1:5000 Jackson ImmunoResearch 715-036-151). Pierce ECL Western Blotting Substrate was used for HRP detection. Signals were detected with a Bio-Rad ChemiDoc MP Imaging System.

P-eIF2a experiments

HCT116 cells were treated with either DMSO, NOC or ST-401 at different times. After drug treatment, one control sample was treated with 500 µM $NaAsO_2$ for 1 h at 37 °C. After this treatment cells were collected using trypsin and centrifuged at 1000 r.p.m. (161 RCF) for 10 min. The cell pellets were resuspended in 100 µL of RIPA buffer with protease inhibitors and incubated in a rocking platform shaker at 4 °C for 60 min. After it, the samples were centrifugated at 12,000 r.p.m. (11,750 RCF) at 4 °C for 30 min. The supernatant was used for a western-blot experiment using a mouse-anti-Phospho-eIF2α (Ser 51, 1:5000, Proteintech 68023-1). To detect primary Ab, we used a donkey-anti-mouse Ab fused to HRP (1:5000 Jackson ImmunoResearch 715-036-151). Pierce ECL Western Blotting Substrate was used for HRP detection. Signals were detected with a Bio-Rad ChemiDoc MP Imaging System.

Autophagy

Flow cytometry: HCT116 cells were treated with either DMSO, NOC or ST-401 for 24 h. After drug treatment, cells were incubated with 50 µM of MDC (Sigma-Aldrich 30432) for 45 min at 4 °C in the dark. After MDC incubation, cells were washed with PBS 3 times, detached using trypsin and centrifuged at 2000 r.p.m. (644 RCF) for 10 min. Cell pellets were washed another 3 times with PBS and resuspended in 1 mL of PBS. Cells were processed by flow cytometry using a BD LSR II Flow Cytometer, and data was analyzed using FlowLogic software. Microscopy: HCT116 cells were treated with either DMSO, NOC or ST-401 for 24 h. After drug treatment, cells were incubated with 50 µM MDC for 15 min at 37 °C in the dark. Cells were then fixed with 4% PFA in PBS at 37 °C for 15 min and permeabilized in 0.5% Triton X-100 for 5 min at room temperature. After a PBS washes, cells were incubated with WGA-594 (Wheat Germ Agglutinin fused to a fluorophore) at RT for 10 min to label the cell membrane. After PBS wash, coverslips were mounted using ProLong® Diamond containing DAPI (Molecular Probes, Eugene, OR) and cured for 24 h. Fluorescent images were collected as 0.5-µm Z-stacks on a Deltavision microscope system (Applied Precision/GEHealthcare, Issaquah, WA) using a 60×1.42 NA lens (Olympus, Tokyo, Japan). Images were deconvolved using SoftWorx 5.0 (Applied Precision/GEHealthcare), and representative images are presented as Maximum intensity Z-projection.

G3BP1

HCT116 cells were treated with either DMSO, NOC or ST-401 for 24 h. After drug treatment, a CTR sample was treated with 500 µM $NaAsO_2$ for 1 h at 37 °C. Cells were then fixed with 4% PFA in PBS at 37 °C for 15 min and permeabilized in 0.5% Triton X-100 for 5 min at room temperature. G3BP1 was labeled using a mouse-anti-G3BP1 (1:250, Proteintech, 66486-1) applied overnight at 4 °C. A donkey-anti-mouse Ab Alexa-fluor-488 (1:500) was used to detect the anti-G3BP1 Ab. After PBS wash, coverslips were mounted using ProLong® Diamond containing DAPI (Molecular Probes, Eugene, OR) and cured for 24 h. Fluorescent images were collected as 0.5-µm Z-stacks on a Deltavision microscope system (Applied Precision/GEHealthcare, Issaquah, WA) using a 60×1.42 NA lens (Olympus, Tokyo, Japan). Images were deconvolved using SoftWorx 5.0 (Applied Precision/ GEHealthcare), and representative images are presented as Maximum intensity Z-projection.

Mitochondria morphology

Cells were plated in 96-well plates with glass bottom from In Vitro Scientific, USA (IVS-P96-1.5H-N). After treatment for 24 h with DMSO, NOC or ST-401, cells were incubated with 100 nM MitoTracker green FM (Invitrogen M7514) for 45 min at 37 °C. After a media wash, fluorescent images of random fields were collected as 0.3-µm Z-stacks using a GE InCell 2500 with a 60× lens. Images were processed using FiJi and analyzed for mitochondrial morphology using the FiJi plugin MitoLoc (a.k.a.MitoMap).

Mitochondrial function

The Cell Mito stress test was employed to assess key metabolic parameters, including Oxygen Consumption Rate (OCR), Extracellular Acidification Rate (ECAR), and ATP production, using the Agilent XFe96 Seahorse analyzer (Agilent Technologies, Wilmington, DE). Cells ($0.75×10^4$) were seeded into a 96-well plate, treated with specific compounds, and incubated for 24 h. OCR and ECAR were measured under basal conditions, and, subsequently, 1 µM oligomycin, 1 µM FCCP, and 1 µM antimycin A/rotenone were added to the cells. Relevant parameters, such as basal and maximal respiration, ATP production, proton leak, non-mitochondrial respiration, and spare respiratory capacity, were calculated in accordance [75]. Data were normalized based on cell numbers determined through microscopy analysis.

Abbreviations

AV	Annexin-V
CIN	Chromosomal instability
DEG	Differentially expressed
ECAR	Extracellular acidification rate

Vicente *et al. Journal of Translational Medicine*   (2024) 22:441

Page 18 of 20

ISR	Integrated stress response
MTs	Microtubules
MTAs	Microtubule targeting agents
MRPs	Mitochondrial ribosomal proteins
MDC	Monodansylcadaverine
NOC	Nocodazole
P-p53	Phosphorylated p53
OXPHOS	Oxidative phosphorylation
OCR	Oxygen consumption rate
PGCC	Polyploid giant cancer cells
PCA	Principal Component Analysis
PI	Propidium iodide
SAC	Spindle assembly checkpoint
TGI	Total growth inhibition
UMAP	Uniform Manifold Approximation and Projection

Supplementary Information

The online version contains supplementary material available at https://doi.org/10.1186/s12967-024-05234-3.

Additional file 1: Additional figures.

Author contributions

JJV and NS designed the study. JJV and KK performed the experiments and acquired the data. JJV, KK, GT, JLMF, YS and NS analyzed the data. JJV, KK, JLMF and NS prepared the figures. JJV and NS supervised the study. JJV and NS drafter the original manuscript. All authors contributed to manuscript editing and writing. All authors read and approved the final manuscript.

Availability of data and materials

All data are available in the main text or the supplementary materials. The raw data related to the scRNAseq will be share upon request to the corresponding authors.

Declarations

Ethics approval and consent to participate
Does not apply.

Consent for publication
Does not apply.

Competing interests
NS is employed by Stella Consulting LLC. The terms of this arrangement have been reviewed and approved by the University of Washington in accordance with its policies governing outside work and financial conflicts of interest in research. All the other authors declare that they have no competing interests.

Author details
[1]Department of Physiology and Biophysics, University of Washington, Health Sciences Building G424, 1705 NE Pacific Str., Seattle, WA 98195-7280, USA. [2]Department of Pharmacology, University of Washington, Health Sciences Center F404A, 1959 NE Pacific Str., Seattle, WA 98195-7280, USA. [3]Department of Biomedical Engineering, Columbia University, New York, NY 10025, USA. [4]Department of Psychiatry and Behavioral Sciences, University of Washington, Seattle, WA 98195, USA.

References

1. Brouhard GJ, Rice LM. Microtubule dynamics: an interplay of biochemistry and mechanics. Nat Rev Mol Cell Biol. 2018;19:451–63.
2. Steinmetz MO, Prota AE. Microtubule-targeting agents: strategies to hijack the cytoskeleton. Trends Cell Biol. 2018;28:776–92.
3. Wordeman L, Vicente JJ. Microtubule targeting agents in disease: classic drugs. Novel Roles Cancers. 2021;13:5650.
4. Duan Y, Liu W, Tian L, Mao Y, Song C. Targeting tubulin-colchicine site for cancer therapy: inhibitors, antibody- drug conjugates and degradation agents. Curr Top Med Chem. 2019;19:1289–304.
5. Sazonova EV, Petrichuk SV, Kopeina GS, Zhivotovsky B. A link between mitotic defects and mitotic catastrophe: detection and cell fate. Biol Direct. 2021;16:25.
6. Jakhar R, Luijten MNH, Wong AXF, Cheng B, Guo K, Neo SP, et al. Autophagy governs protumorigenic effects of mitotic slippage-induced senescence. Mol Cancer Res. 2018;16:1625–40.
7. Mitchison TJ. The proliferation rate paradox in antimitotic chemotherapy. Mol Biol Cell. 2012;23:1–6.
8. Field JJ, Kanakkanthara A, Miller JH. Microtubule-targeting agents are clinically successful due to both mitotic and interphase impairment of microtubule function. Bioorg Med Chem. 2014;22:5050–9.
9. Komlodi-Pasztor E, Sackett DL, Fojo AT. Inhibitors targeting mitosis: tales of how great drugs against a promising target were brought down by a flawed rationale. Clin Cancer Res. 2012;18:51–63.
10. Was H, Borkowska A, Olszewska A, Klemba A, Marciniak M, Synowiec A, et al. Polyploidy formation in cancer cells: how a Trojan horse is born. Semin Cancer Biol. 2022;81:24–36.
11. Fei F, Zhang D, Yang Z, Wang S, Wang X, Wu Z, et al. The number of polyploid giant cancer cells and epithelial-mesenchymal transition-related proteins are associated with invasion and metastasis in human breast cancer. J Exp Clin Cancer Res. 2015;34:158.
12. Niu N, Mercado-Uribe I, Liu J. Dedifferentiation into blastomere-like cancer stem cells via formation of polyploid giant cancer cells. Oncogene. 2017;36:4887–900.
13. Shabo I, Svanvik J, Lindström A, Lechertier T, Trabulo S, Hulit J, et al. Roles of cell fusion, hybridization and polyploid cell formation in cancer metastasis. World J Clin Oncol. 2020;11:121–35.
14. Zhang S, Mercado-Uribe I, Xing Z, Sun B, Kuang J, Liu J. Generation of cancer stem-like cells through the formation of polyploid giant cancer cells. Oncogene. 2013;33:116–28.
15. Zhang S, Mercado-Uribe I, Liu J. Tumor stroma and differentiated cancer cells can be originated directly from polyploid giant cancer cells induced by paclitaxel. Int J Cancer. 2013;134:508–18.
16. Zhou X, Zhou M, Zheng M, Tian S, Yang X, Ning Y, et al. Polyploid giant cancer cells and cancer progression. Front Cell Dev Biol. 2022;10:1017588.
17. Cherry AE, Haas BR, Naydenov AV, Fung S, Xu C, Swinney K, et al. ST-11: a new brain-penetrant microtubule-destabilizing agent with therapeutic potential for glioblastoma multiforme. Mol Cancer Ther. 2016;15:2018–29.
18. Diaz P, Horne E, Xu C, Hamel E, Wagenbach M, Petrov RR, et al. Modified carbazoles destabilize microtubules and kill glioblastoma multiform cells. Eur J Med Chem. 2018;159:74–89.
19. Fung S, Xu C, Hamel E, Wager-Miller JB, Woodruff G, Miller A, et al. Novel indole-based compounds that differentiate alkylindole-sensitive receptors from cannabinoid receptors and microtubules: characterization of their activity on glioma cell migration. Pharmacol Res. 2017;115:233–41.
20. Horne EA, Diaz P, Cimino PJ, Jung E, Xu C, Hamel E, et al. A brain-penetrant microtubule-targeting agent that disrupts hallmarks of glioma tumorigenesis. Neurooncol Adv. 2021;3: vdaa165.

Vicente *et al. Journal of Translational Medicine*   (2024) 22:441

Page 19 of 20

21. Sharma SV, Haber DA, Settleman J. Cell line-based platforms to evaluate the therapeutic efficacy of candidate anticancer agents. Nat Rev Cancer. 2010;10:241–53.

22. Ertych N, Stolz A, Stenzinger A, Weichert W, Kaulfuß S, Burfeind P, et al. Increased microtubule assembly rates influence chromosomal instability in colorectal cancer cells. Nat Cell Biol. 2014;16:779–91.

23. Thompson SL, Compton DA. Chromosome missegregation in human cells arises through specific types of kinetochore–microtubule attachment errors. Proc Natl Acad Sci. 2011;108:17974–8.

24. Yamaguchi H, Chen J, Bhalla K, Wang H-G. Regulation of Bax activation and apoptotic response to microtubule-damaging agents by p53 transcription-dependent and -independent pathways. J Biol Chem. 2004;279:39431–7.

25. Paull KD, Lin CM, Malspeis L, Hamel E. Identification of novel antimitotic agents acting at the tubulin level by computer-assisted evaluation of differential cytotoxicity data. Cancer Res. 1992;52:3892–900.

26. Jordan MA, Thrower D, Wilson L. Effects of vinblastine, podophyllotoxin and nocodazole on mitotic spindles : implications for the role of microtubule dynamics in mitosis. J Cell Sci. 1992;102:401–16.

27. Tsuiki H, Nitta M, Tada M, Inagaki M, Ushio Y, Saya H. Mechanism of hyperploid cell formation induced by microtubule inhibiting drug in glioma cell lines. Oncogene. 2001;20:420–9.

28. Verdoodt B. Induction of polyploidy and apoptosis after exposure to high concentrations of the spindle poison nocodazole. Mutagenesis. 1999;14:513–20.

29. Coward J, Harding A. Size does matter: why polyploid tumor cells are critical drug targets in the war on cancer. Front Oncol. 2014;4:123.

30. Icha J, Weber M, Waters JC, Norden C. Phototoxicity in live fluorescence microscopy, and how to avoid it. BioEssays. 2017;39:1700003.

31. Jung S, Jeong H, Yu S-W. Autophagy as a decisive process for cell death. Exp Mol Med. 2020;52:921–30.

32. Biederbick A, Kern HF, Elsässer HP. Monodansylcadaverine (MDC) is a specific in vivo marker for autophagic vacuoles. Eur J Cell Biol. 1995;66:3–14.

33. Button RW, Roberts SL, Willis TL, Hanemann CO, Luo S. Accumulation of autophagosomes confers cytotoxicity. J Biol Chem. 2017;292:13599–614.

34. Chen J. The cell-cycle arrest and apoptotic functions of p53 in tumor initiation and progression. Cold Spring Harb Perspect Med. 2016;6: a026104.

35. Hinchcliffe EH, Day CA, Karanjeet KB, Fadness S, Langfald A, Vaughan KT, et al. Chromosome missegregation during anaphase triggers p53 cell cycle arrest through histone H3.3 Ser31 phosphorylation. Nat Cell Biol. 2016;18:668–75.

36. Cao J, Spielmann M, Qiu X, Huang X, Ibrahim DM, Hill AJ, et al. The single-cell transcriptional landscape of mammalian organogenesis. Nature. 2019;566:496–502.

37. Gay DA, Yen TJ, Lau JT, Cleveland DW. Sequences that confer beta-tubulin autoregulation through modulated mRNA stability reside within exon 1 of a beta-tubulin mRNA. Cell. 1987;50:671–9.

38. Lin Z, Gasic I, Chandrasekaran V, Peters N, Shao S, Mitchison TJ, et al. TTC5 mediates autoregulation of tubulin via mRNA degradation. Science. 2020;367:100–4.

39. van Riggelen J, Yetil A, Felsher DW. MYC as a regulator of ribosome biogenesis and protein synthesis. Nat Rev Cancer. 2010;10:301–9.

40. Kambhatla N, Leen TK. Dimension reduction by local principal component analysis. Neural Comput. 1997;9:1493–516.

41. Traag VA, Waltman L, van Eck NJ. From Louvain to Leiden: guaranteeing well-connected communities. Sci Rep. 2019;9:5233.

42. Subramanian A, Tamayo P, Mootha VK, Mukherjee S, Ebert BL, Gillette MA, et al. Gene set enrichment analysis: a knowledge-based approach for interpreting genome-wide expression profiles. Proc Natl Acad Sci. 2005;102:15545–50.

43. Pakos-Zebrucka K, Koryga I, Mnich K, Ljujic M, Samali A, Gorman AM. The integrated stress response. EMBO Rep. 2016;17:1374–95.

44. Kedersha N, Stoecklin G, Ayodele M, Yacono P, Lykke-Andersen J, Fritzler MJ, et al. Stress granules and processing bodies are dynamically linked sites of mRNP remodeling. J Cell Biol. 2005;169:871–84.

45. Yang P, Mathieu C, Kolaitis R-M, Zhang P, Messing J, Yurtsever U, et al. G3BP1 is a tunable switch that triggers phase separation to assemble stress granules. Cell. 2020;181:325-345.e28.

46. McEwen E, Kedersha N, Song B, Scheuner D, Gilks N, Han A, et al. Heme-regulated Inhibitor Kinase-mediated phosphorylation of eukaryotic translation initiation factor 2 inhibits translation, induces stress granule formation, and mediates survival upon arsenite exposure. J Biol Chem. 2005;280:16925–33.

47. Kummer E, Ban N. Mechanisms and regulation of protein synthesis in mitochondria. Nat Rev Mol Cell Biol. 2021;22:307–25.

48. Vowinckel J, Hartl J, Butler R, Ralser M. MitoLoc: A method for the simultaneous quantification of mitochondrial network morphology and membrane potential in single cells. Mitochondrion. 2015;24:77–86.

49. Jordan MA, Wilson L. Microtubules as a target for anticancer drugs. Nat Rev Cancer. 2004;4:253–65.

50. Kaul R, Risinger AL, Mooberry SL. Microtubule-targeting drugs: more than antimitotics. J Nat Prod. 2019;82:680–5.

51. Gascoigne KE, Taylor SS. Cancer cells display profound intra- and interline variation following prolonged exposure to antimitotic drugs. Cancer Cell. 2008;14:111–22.

52. Goodson HV, Jonasson EM. Microtubules and microtubule-associated proteins. Cold Spring Harb Perspect Biol. 2018;10: a022608.

53. Moujaber O, Stochaj U. The cytoskeleton as regulator of cell signaling pathways. Trends Biochem Sci. 2020;45:96–107.

54. Kothari A, Hittelman WN, Chambers TC. Cell cycle-dependent mechanisms underlie vincristine-induced death of primary acute lymphoblastic leukemia cells. Can Res. 2016;76:3553–61.

55. Delgado M, Urbaniak A, Chambers TC. Contrasting effects of microtubule destabilizers versus stabilizers on induction of death in G1 phase of the cell cycle. Biochem Pharmacol. 2019;162:213–23.

56. Vicente JJ, Wordeman L. The quantification and regulation of microtubule dynamics in the mitotic spindle. Curr Opin Cell Biol. 2019;60:36–43.

57. Bharadwaj D, Mandal M. Senescence in polyploid giant cancer cells: a road that leads to chemoresistance. Cytokine Growth Factor Rev. 2020;52:68–75.

58. Telleria CM. Repopulation of ovarian cancer cells after chemotherapy. Cancer Growth Metastasis. 2013;6:CGM.S11333.

59. Hofmann S, Cherkasova V, Bankhead P, Bukau B, Stoecklin G. Translation suppression promotes stress granule formation and cell survival in response to cold shock. Mol Biol Cell. 2012;23:3786–800.

60. Tian X, Zhang S, Zhou L, Seyhan AA, Hernandez Borrero L, Zhang Y, et al. Targeting the integrated stress response in cancer therapy. Front Pharmacol. 2021;12: 747837.

61. Jana S, Deo R, Hough RP, Liu Y, Horn JL, Wright JL, et al. mRNA translation is a therapeutic vulnerability necessary for bladder epithelial transformation. JCI Insight. 2021;6: e144920.

62. Parker AL, Kavallaris M, McCarroll JA. Microtubules and their role in cellular stress in cancer. Front Oncol. 2014;4:153.

63. Morava E, Kozicz T. Mitochondria and the economy of stress (mal)adaptation. Neurosci Biobehav Rev. 2013;37:668–80.

64. Hanahan D, Weinberg RA. Hallmarks of cancer: the next generation. Cell. 2011;144:646–74.

65. Vasan K, Werner M, Chandel NS. Mitochondrial metabolism as a target for cancer therapy. Cell Metab. 2020;32:341–52.

66. Villalpando-Rodriguez GE, Gibson SB. Reactive oxygen species (ROS) regulates different types of cell death by acting as a rheostat. Oxid Med Cell Longev. 2021;2021:1–17.

67. Huang G, Li H, Zhang H. Abnormal expression of mitochondrial ribosomal proteins and their encoding genes with cell apoptosis and diseases. Int J Mol Sci. 2020;21:8879.

68. Kim H-J, Maiti P, Barrientos A. Mitochondrial ribosomes in cancer. Semin Cancer Biol. 2017;47:67–81.

69. Vivier E, Raulet DH, Moretta A, Caligiuri MA, Zitvogel L, Lanier LL, et al. Innate or adaptive immunity? The example of natural killer cells. Science. 2011;331:44–9.

70. Wu S-Y, Fu T, Jiang Y-Z, Shao Z-M. Natural killer cells in cancer biology and therapy. Mol Cancer. 2020;19:120.

71. Huntington ND, Cursons J, Rautela J. The cancer-natural killer cell immunity cycle. Nat Rev Cancer. 2020;20:437–54.

72. Minetto P, Guolo F, Pesce S, Greppi M, Obino V, Ferretti E, et al. Harnessing NK cells for cancer treatment. Front Immunol. 2019;10:2836.

Vicente *et al. Journal of Translational Medicine*   (2024) 22:441

Page 20 of 20

73. Mackenzie KJ, Carroll P, Martin C-A, Murina O, Fluteau A, Simpson DJ, et al. cGAS surveillance of micronuclei links genome instability to innate immunity. Nature. 2017;548:461–5.
74. Vanpouille-Box C, Alard A, Aryankalayil MJ, Sarfraz Y, Diamond JM, Schneider RJ, et al. DNA exonuclease Trex1 regulates radiotherapy-induced tumour immunogenicity. Nat Commun. 2017;8:15618.
75. Tan B, Xiao H, Li F, Zeng L, Yin Y. The profiles of mitochondrial respiration and glycolysis using extracellular flux analysis in porcine enterocyte IPEC-J2. Animal Nutrition. 2015;1:239–43.

Publisher's Note